UCRL-16999

University of California

Ernest O. Lawrence Radiation Laboratory

THE MAGNETIC MOMENT OF PLUTONIUM-239

TWO-WEEK LOAN COPY

This is a Library Circulating Copy which may be borrowed for two weeks. For a personal retention copy, call Tech. Info. Division, Ext. 5545

DISCLAIMER

This document was prepared as an account of work sponsored by the United States Government. While this document is believed to contain correct information, neither the United States Government nor any agency thereof, nor the Regents of the University of California, nor any of their employees, makes any warranty, express or implied, or assumes any legal responsibility for the accuracy, completeness, or usefulness of any information, apparatus, product, or process disclosed, or represents that its use would not infringe privately owned rights. Reference herein to any specific commercial product, process, or service by its trade name, trademark, manufacturer, or otherwise, does not necessarily constitute or imply its endorsement, recommendation, or favoring by the United States Government or any agency thereof, or the Regents of the University of California. The views and opinions of authors expressed herein do not necessarily state or reflect those of the United States Government or any agency thereof or the Regents of the University of California.

UCRL-16999

UNIVERSITY OF CALIFORNIA

Lawrence Radiation Laboratory
Berkeley, California

AEC Contract No. W-7405-eng-48

THE MAGNETIC MOMENT OF PLUTONIUM-239

John Faust

(Ph.D. Thesis)

August 4, 1966

THE MAGNETIC MOMENT OF PLUTONIUM-239

John Faust

Contents

Abstract iv

I. Introduction 1

II. Theory

A. Introduction 3

B. Atomic Spectra 3

C. The hfs Perturbation 5

D. Configuration Mixing and Core Polarization 8

E. Magnetic Field 9

F. Second-Order Effects 11

G. Nuclear Structure 13

H. Transition Probabilities 20

III. Apparatus

A. Introduction 26

B. Overall Design and Dimensions 26

C. Oven Loaders and Beam Sources 26

D. Magnet System 31

E. Vacuum System 33

F. Radio-Frequency System 34

G. Detection 36

IV. Experimental Procedure

A. Introduction 41

B. Isotope Production 41

C. Beam Production 43

V. Experimental Results 47

A. Plutonium-239 47

B. Four- and Six-Quantum Transitions in W^{185} and W^{187}, and Pu^{241} 49

Acknowledgments 55

List of Illustrations 56

List of Tables 57

References 58

ABSTRACT

The triple-loop technique of atomic-beam magnetic resonance has been used to determine the magnetic moment of plutonium-239 directly. The final measurement was carried out at a magnetic field of 720 gauss and the magnetic moment was found to be

$$\mu_I = +\ 0.200(4)\ \text{nm (corrected)} \quad ,$$

where the sign is measured to be positive.

Hyperfine-structure measurements on plutonium-241 and tungsten-185 and tungsten-187 were attempted. These experiments involved the observation of four- and six-quantum transitions because of the inverted level ordering which was caused by the unusually large values of the quadrupole moments of all of these isotopes.

I. INTRODUCTION

Of the many ways to study nuclear structure, the atomic beam experiment is capable of giving the least ambiguous results because of the relative purity of an environment over which one has a high degree of control. There are no crystal fields, no nearest-neighbor interactions, and few collisions at the high vacuum used.

The use of a calibration isotope for which atomic and nuclear constants are well known, and highly accurate frequency measuring devices combined with the possibility, under the right circumstances, of observing narrow linewidths, results in the opportunity of measuring nuclear and atomic constants to a high degree of accuracy. The triple-loop technique makes possible the observation of $\Delta m_I = \pm 1$, $\Delta m_J = 0$ transitions that previously were not observable in atomic beam experiments even though the transitions are permitted by the strong-field selection rules.

The nuclear constants of Pu^{239} have been the subject of measurement since 1954 when Van den Berg et al. measured the nuclear spin and found it to be 1/2 (VAN-54). Also in 1954 the magnetic moment was inferred from a paramagnetic resonance experiment by Bleaney et al. to be $\pm$ 0.4(2) nm (BLE-54). In 1958, Marrus et al. measured an extremely small value for the hyperfine-structure constant, $\Delta\nu$, of 5.2 MHz, and inferred from this a small moment of 0.02 nm (HUB-58). Champeau, Gerstenkorn, and others have obtained, since 1960, better and better values for the hyperfine structures of many of the J states in the spectrum of Pu-I and Pu-II by optical spectroscopic techniques (CHA-60) (GER-62); from these hfs values, Bauche and Judd were able to predict (BAU-64) that the magnetic moment of Pu^{239} should be

$$\mu_I = 0.17(4) \text{ nm (theoretical;hfs)} .$$

The directly measured value of $\mu_I = 0.200(4)$ nm (experimental,corr.) is within the limits of error set by their calculation.

The values of the nuclear electric quadrupole moments of Pu^{241} and of W^{185} and W^{187} are so large that the only observable transitions were four- and six-quantum transitions whose transition probabilities decreased so rapidly with increasing field that no appreciable splitting from the Zeeman frequencies was observed before the resonances disappeared. As a result, the hyperfine separations of these three isotopes could not be obtained.

Table I-I. Other measurements of Pu^{239}.

Group	Spin	Nuclear moment values (nm)	Reference
Van den Berg et al.	1/2		VAN-54
Korostyleva et al.	1/2		KOR-55
Bleaney et al.		0.4(2)	BLE-54
Hubbs et al.		0.021	HUB-58
Champeau & Gerstenkorn		0.27(6)	CHA-60
Gerstenkorn		0.21(6)	GER-62
Korostyleva		0.15(4)	KOR-62
Berthelot		0.207(33)	BER-63
Korostyleva		0.19(4)	KOR-66

II. THEORY

A. Introduction

The theory of atomic and nuclear structure requires solving Schrödinger's equation for a Hamiltonian that includes terms for all the interactions in which either one is interested, or one can think of as being applicable. Since most of the terms of the Hamiltonian are either quite complex mathematically, or not separable, or both, one must usually resort to some kind of perturbation theory in order to get values for observable energies to any reasonable accuracy. "Resort" is perhaps not the proper word to use, since the results of using perturbation theory are often extremely accurate. The procedure is to use some "simple" Hamiltonian which is separable in the coordinates of interest, find eigenenergies and eigenfunctions for this Hamiltonian, and use these energies and functions as a zero-order starting point. Then one assigns to any change in the energy or eigenfunction a continuously varying parameter which corresponds physically to "turning on" the perturbation, puts the "perturbed" energies and wavefunctions back into the Schrödinger equation, and finally solves for the perturbation energies and wavefunctions in terms of their zero-order values and the initial conditions. This procedure is carried out for all levels of perturbation, by use of the results of the previous calculation as "zero-order" solutions (CON-35).

B. Atomic Spectra

The Hamiltonian of a free atom in a magnetic field is

$$\mathcal{H} = \sum_i \left\{ \frac{p_i^2}{2m} + U_i(\underset{\sim}{r}_i) - \frac{Ze^2}{r_i} + \sum_{j>i} \frac{e^2}{r_{ij}} - U_i(\underset{\sim}{r}_i) + \xi(\underset{\sim}{r}_i)\, \underset{\sim}{\ell}_i \cdot \underset{\sim}{s}_i \right\} + \mathcal{H}_{hfs} + \mathcal{H}_m \tag{II-1}$$

$$= \mathcal{H}_o + \mathcal{H}_t + \mathcal{H}_{fs} + \mathcal{H}_{hfs} + \mathcal{H}_m \quad ; \tag{II-2}$$

$$\mathcal{H}_o = \sum_i \left\{ \frac{p_i^2}{2m} + U_i(\underset{\sim}{r}_i) \right\} \qquad \text{(II-3)}$$

is the spherically symmetric approximation to

$$\sum_i \left\{ \frac{p_i^2}{2m} - \frac{Ze^2}{r_i} + \sum_{j>i} \frac{e^2}{r_{ij}} \right\} , \qquad \text{(II-4)}$$

and gives rise to the zero-order energy levels of the atom. These levels have an energy characterized by n and ℓ, the principal quantum number and the orbital quantum number respectively. The perturbation which gives rise to the "terms" of optical spectroscopy is

$$\mathcal{H}_t = \sum_i \left\{ - \frac{Ze^2}{r_i} + \sum_{j>i} \frac{e^2}{r_{ij}} - U_i(\underset{\sim}{r}_i) \right\} . \qquad \text{(II-5)}$$

It is the non-spherically-symmetric part of the interelectron repulsion.

$$\mathcal{H}_{fs} = \sum_i \xi(\underset{\sim}{r}_i)\ \underset{\sim}{\ell}_i \cdot \underset{\sim}{s}_i \qquad \text{(II-6)}$$

gives rise to the fine-structure levels; $\mathcal{H}_{hfs}$ and $\mathcal{H}_m$ give rise to the hyperfine structure levels and the magnetic field effects respectively.

When $\mathcal{H}_t \gg \mathcal{H}_{fs}$ the individual $\underset{\sim}{\ell}_i$'s and $\underset{\sim}{s}_i$'s of the electrons couple to a total $\underset{\sim}{L}$ and a total $\underset{\sim}{S}$ which then couple to form $\underset{\sim}{J}$. This is called LS or Russell-Saunders coupling, a condition which obtains for most light elements and at least approximately for many heavier ones. When $\mathcal{H}_{fs} \gg \mathcal{H}_t$ the individual $\underset{\sim}{\ell}_i$ and $\underset{\sim}{s}_i$ of each electron couple directly to an individual $\underset{\sim}{j}_i$, whereupon all the $\underset{\sim}{j}_i$'s couple to $\underset{\sim}{J}$ of the atom. This is called j-j coupling and it is characteristic of some heavy atoms and of nuclei in general.

Usually $\mathcal{H}_{hfs} \ll \mathcal{H}_{fs}$ or $\mathcal{H}_t$. Then the different energy levels associated with different J values are far apart. J is a good quantum number and the hfs separation $\Delta\nu$ is easily calculated.

Application of the fine-structure perturbation splits each term into $(2S + 1)$ or $(2L + 1)$ levels, whichever number is smaller. The hyperfine-structure perturbation in turn splits each of these J levels into $(2J + 1)$ or $(2I + 1)$ levels, whichever is smaller. These levels are characterized by values of F. The application of a magnetic field, which is the only truly controllable perturbation discussed so far, further splits each of these levels into $(2F + 1)$ more levels characterized by values of m_F. A schematic diagram showing relative energy splittings and degeneracies is shown in Fig. II-1. Figure II-2 shows fine, hyperfine, and magnetic levels more closely to scale, to illustrate the degree of inequality in the strengths of the various perturbation terms.

C. The hfs Perturbation

For the case I or $J < 1$, $\mathcal{H}_{hfs} = - \underset{\sim}{\mu}_I \cdot \underset{\sim}{H}_J$, which, for diagonal matrix elements, can be written as $a\underset{\sim}{I}\cdot\underset{\sim}{J}$, where

$$a = \frac{1}{IJ} \langle II|\underset{\sim}{\mu}_I|II\rangle\langle JJ|\underset{\sim}{H}_J|JJ\rangle \quad .$$

This separation can be done because $\underset{\sim}{H}_J$ is a "T"-type operator with respect to $\underset{\sim}{J}$, and $\underset{\sim}{\mu}_I$ has the same relationship to $\underset{\sim}{I}$ (CON-35, p. 59).

$\langle II|\underset{\sim}{\mu}_I|II\rangle \equiv \mu_I$, the measured magnetic moment, whereas the matrix element, $\langle JJ|\underset{\sim}{H}_J|JJ\rangle$, depends on the coupling rule for the electronic angular momentum vectors. For a single non-s electron,

$$\underset{\sim}{H}_J = \frac{e\underset{\sim}{v} \times \underset{\sim}{r}}{cr^3} + \frac{\underset{\sim}{\mu} - 3(\underset{\sim}{\mu}\cdot\hat{r})\hat{r}}{r^3} \qquad \text{(II-7)}$$

$$= - \mu_o \frac{2\underset{\sim}{\ell}}{r^3} + \frac{2\mu_o}{r^3} [\underset{\sim}{s} - 3(\underset{\sim}{s}\cdot\hat{r})\hat{r}] \quad , \qquad \text{(II-8)}$$

where $\underset{\sim}{v}$ is the velocity and $\hat{r}$ is a unit vector in the direction of $\underset{\sim}{r}$.

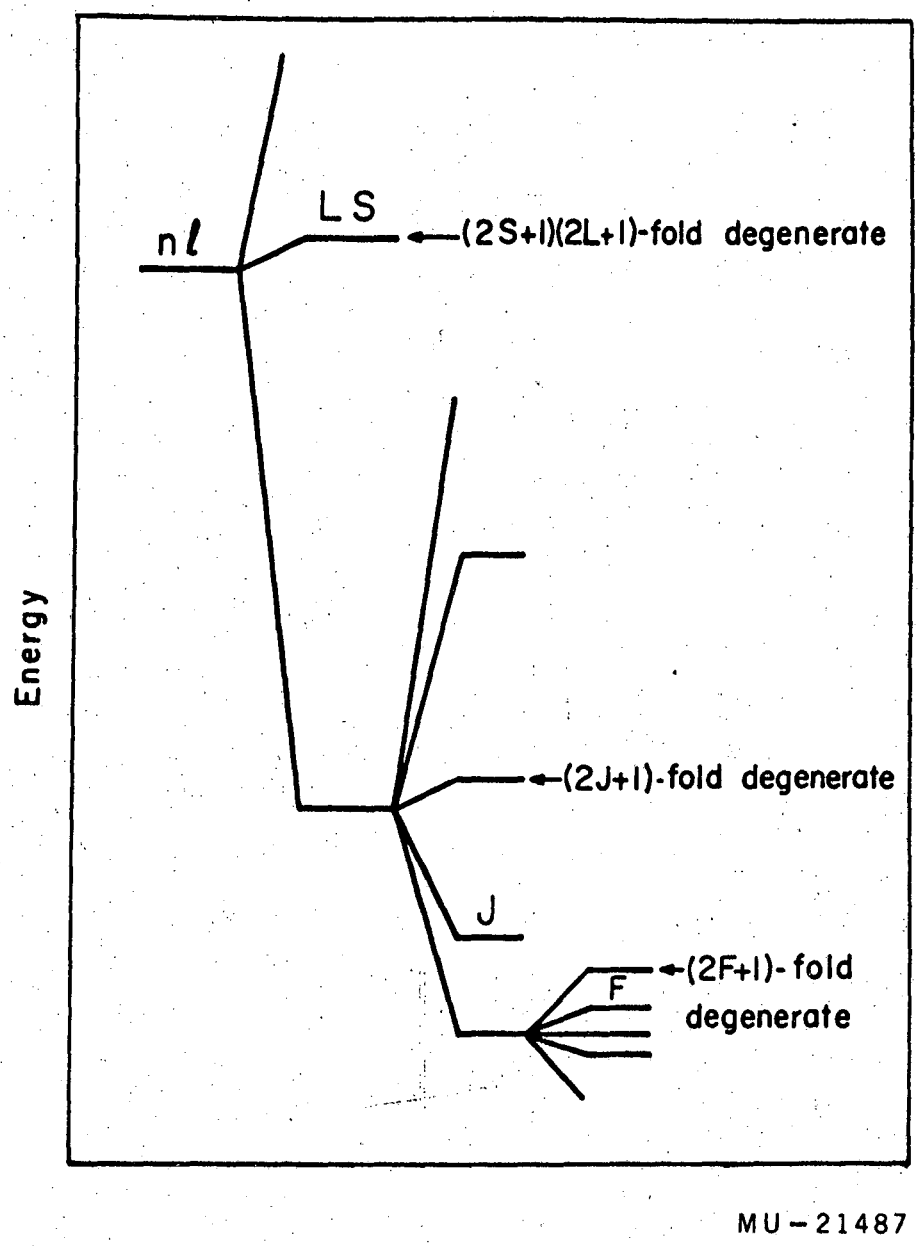

Fig. II-1 Relative energy splittings and degeneracies.

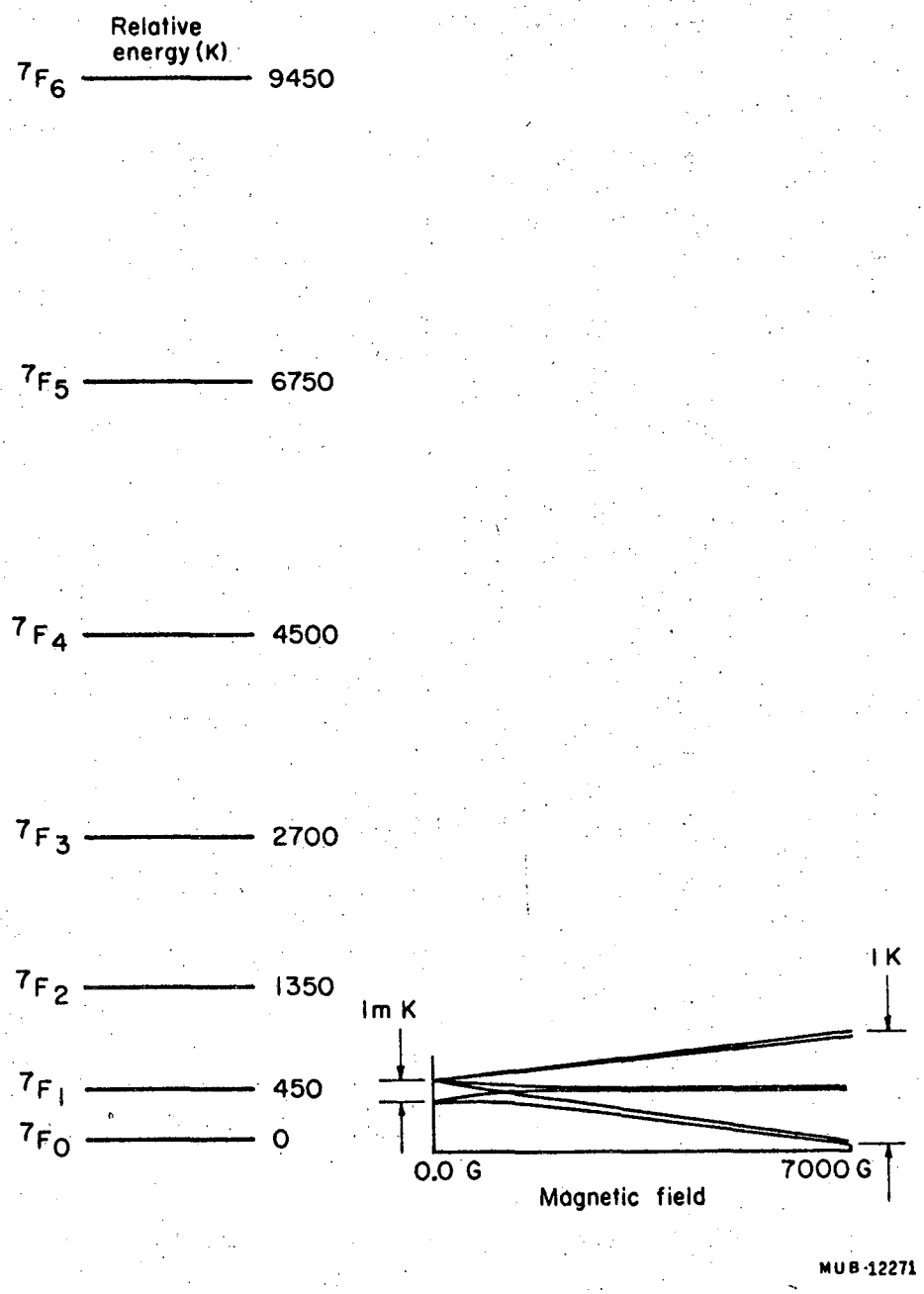

Fig. II-2 Fine, hyperfine, and magnetic splitting energy levels.

For the case of many equivalent electrons, the matrix elements have been evaluated (HUB-58) to be

$$\langle LSJm_J|\underset{\sim}{H}|LSJm_J\rangle = \langle LSJ\|\underset{\sim}{J}\|LSJ\rangle(A\ \underset{\sim}{L}\cdot\underset{\sim}{J}/J^2) \quad .$$

The constant A can be evaluated for a level ^7F_J of the configuration $(5f)^6$ to be

$$A(J) = \frac{\mu_I}{I}\,\mu_o^2\,\langle r^{-3}\rangle\,\frac{[J(J+1)+58]}{90} \qquad \text{(II-9)}$$

for pure LS coupling (MAR-60). When neither $\mathcal{H}_t \ll \mathcal{H}_{fs}$ nor $\mathcal{H}_t \gg \mathcal{H}_{fs}$, one has neither j-j nor LS coupling; the wave functions are mixtures of wave functions between LS and j-j functions. In this case A(J) is altered by an amount equal to the ratio of the matrix elements of the sum of numerators of Eq. (II-8) (for each electron) between the real (mixed) wave functions and the pure LS wave functions. The effect of this is to multiply A(J) by a factor P(J), which is a function of the particular mixing wave functions and their expansion coefficients (BAU-64).

D. Configuration Mixing and Core Polarization

Because s electrons have a very large probability of being near the nucleus and having a large interaction with it, even small admixtures of s-wave functions will have a large effect on the value of A(J) (JUD-63). For an s electron the Hamiltonian (II-7) vanishes and it must be replaced with a δ function (which of course vanishes for non-s electrons):

$$\underset{\sim}{H}_J(s) = -\,2\mu_o^2\,g_I'\,\frac{8\pi}{3}\,\Sigma\,\delta(\underset{\sim}{r}_i)\underset{\sim}{s}_i \quad . \qquad \text{(II-10)}$$

The s electrons interact with the 5f electrons in the unfilled shell by means of the term e^2/r_{ij} in the Hamiltonian (II-5). The contribution to the hyperfine structure of an electron originally in the shell $(ns)^2$, which is excited into a higher s shell (n's), leaving (ns), is

$$\Delta A = 2(1 - g_J)\,\frac{8\pi}{3}\,(2\mu_o^2\ g_I')\sum_{n'} R^3(5fns,\ n's5f)\,\frac{\psi_{ns}(0)\psi_{n's}(0)}{7W(ns,\ n's)}\ , \qquad \text{(II-11)}$$

where the Slater integral, which determines the mixing, is $R^3(5fns,\ n's5f)$, and $W(ns,\ n's)$ is the energy difference between the two s levels.

Actually the sign of the correction calculated in this way is wrong for the most obvious mechanism to change A(J), that is, to excite a (7s) electron to an (8s) shell (MAR-60). If other mechanisms are tried, such as (7s) to (9s) or (10s) the contributions are also of the wrong sign although small; (6s) or (5s) to (8s) would give contributions of the correct sign, but the magnitude is much too small because of the large value of W(6s, 8s) in the denominator of (II-11) (BAU-64). Watson and Freeman have shown that the spin density for s electrons in a filled shell is different for the two electrons, one of which has $m_s = -1/2$, the other $m_s = +1/2$ (WAT-60). The net spin density at the nucleus is not zero and the paired s electrons <u>can</u> contribute to the hyperfine structure.

E. Magnetic Field

The interaction of the external magnetic field with the magnetic moment of the atom is

$$\mathcal{H}_m^1 = (-\,\underset{\sim}{\mu}_L - \underset{\sim}{\mu}_S)\cdot H_{ext} \qquad \text{(II-12)}$$

$$= -\,\mu_o(\underset{\sim}{L}g_L + \underset{\sim}{S}g_S)\cdot H_{ext}\ . \qquad \text{(II-13)}$$

$\mathcal{H}_m^1$ is not diagonal in the $|J,m_J\rangle$ scheme, but it is in the $|m_S,m_L\rangle$ scheme. However, the off-diagonal elements in the $|J,m_J\rangle$ scheme are proportional to the field and are small for very low fields. That is, for very low fields, $\underset{\sim}{L}$ and $\underset{\sim}{S}$ couple to $\underset{\sim}{J}$ to a high degree of accuracy and the matrix of $\mathcal{H}_m^1$ is "nearly" diagonal.

The nucleus does not contribute much magnetic moment, but the amount of angular momentum contributed is on the same order as that of the electrons. The effect of considering the nuclear angular momentum can be seen in the energy levels calculated at low fields. The Hamiltonian

$$\begin{aligned} \mathcal{H}_m^2 &= (-\underset{\sim}{\mu}_J - \underset{\sim}{\mu}_I)\cdot\underset{\sim}{H}_{ext} \\ &= -\mu_o(\underset{\sim}{J}g_J + \underset{\sim}{I}g_I)\cdot\underset{\sim}{H}_{ext} \end{aligned} \qquad \text{(II-14)}$$

is not diagonal in the $|Fm_F\rangle$ scheme; however, the off-diagonal terms are small for very low fields and can be ignored. The diagonal matrix elements are

$$\begin{aligned} \langle Fm_F|-\mu_o(g_J J_z + g_I I_z)H_z|Fm_F\rangle &= -\mu_o\Big[\frac{F(F+1)+J(J+1)-I(I+1)}{2F(F+1)}\,g_J \\ &\quad + \frac{F(F+1)+I(I+1)-J(J+1)}{2F(F+1)}\,g_I\Big]m_F H_z \qquad \text{(II-15)} \\ &= -g_F\mu_o H_z m_F \quad . \end{aligned}$$

Since $g_I \ll g_J$, we find that

$$g_F \approx g_J\,\frac{F(F+1)+J(J+1)-I(I+1)}{2F(F+1)} \qquad \text{(II-16)}$$

and the energies are different for each different F level, with a linear field dependence proportional to the field times the component of total angular momentum F along the field. The proportionality factor is g_J times a function of I, J, and F, instead of just g_J.

The off-diagonal terms in the $|m_I m_J\rangle$ scheme are zero and $\mathcal{H}_m^2$ is diagonal, with matrix elements

$$\langle m_I m_J|\mathcal{H}_m^2|m_I m_J\rangle = -g_J\mu_o m_J H_z - g_I\mu_o m_I H_z \quad , \qquad \text{(II-17)}$$

which are linear in the field. These two formulae, (II-15) and (II-17), allow one to draw a qualitative picture of the field dependence of all

the energy levels in a given F multiplet. An additional rule which is helpful in making the diagram is that lines of the same value of m_F can never cross.

A quantitative description is much harder to obtain at intermediate fields when none of the matrix elements is small in either representation. A Hamiltonian matrix which is (2I + 1)- or (2J + 1)-dimensional (whichever is smaller) must be diagonalized. This is not possible analytically when I and J are both greater than 1/2. It can be done numerically, and a computer program, F2-94, has been set up for the IBM 7094 to do this.

For the case in which I or J = 1/2 (as in Pu^{239}: I = 1/2, J = 1, 2) the matrix is two-dimensional and the equation is quadratic. An analytic solution is called the Breit-Rabi formula (BRE-31):

$$W(F,M) = -\frac{h\Delta\nu}{2(2I+1)} - g_I\mu_o HM \pm \frac{h\Delta\nu}{2}\left(1 + \frac{4Mx}{2I+1} + x^2\right)^{1/2} \qquad \text{(II-18)}$$

$$x = H(g_I - g_J)\mu_o/h\Delta\nu \qquad \text{for} \qquad (J = 1/2) \quad .$$

The positive square root is for the value of $F = I + J$, the negative for $F = |I - J|$. For $I = 1/2$ interchange I and J everywhere in the above formula. A diagram of the energy levels for a system with $I = 1/2$, $J = 1$ is given in Fig. II-3.

F. Second-Order Effects

The values of the energy levels used to determine A and g_I are affected not only by the levels of the same m_F from the other F levels in the same F multiplet, but also by the levels of the same m_F from different J levels in the same multiplet and J levels arising from other configurations. The amount of perturbation can be calculated by second-order perturbation theory, but it is a difficult job to do in detail. Order-of-magnitude estimates are usually sufficient. The correction to g_I is

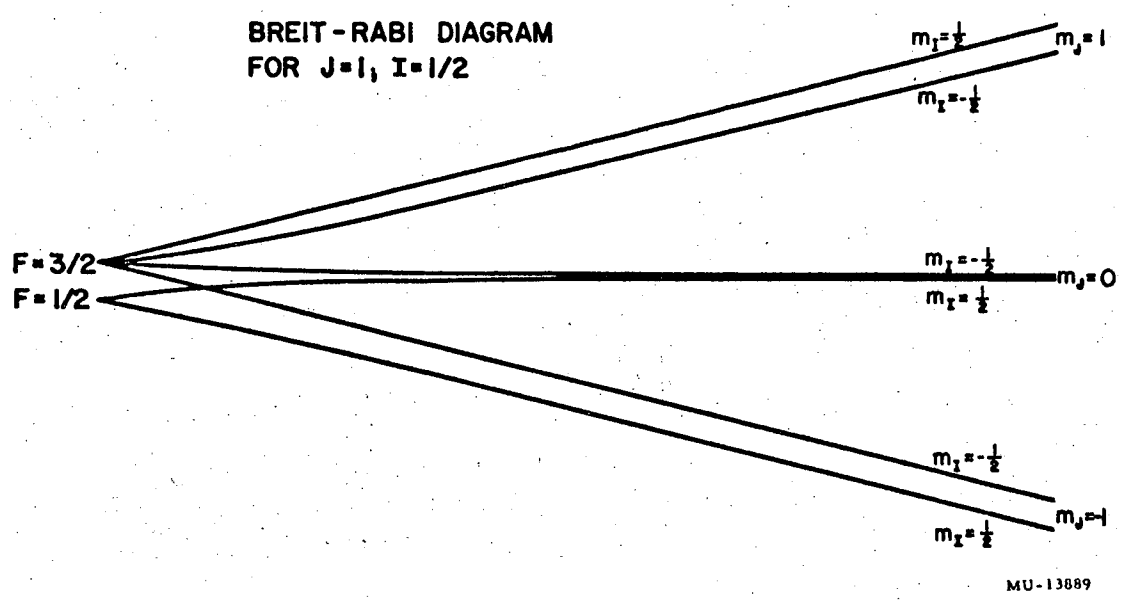

Fig. II-3 Energy levels for Pu^{239} in a magnetic field.

$$\Delta g_I \mu_o H \approx \frac{2W_{hfs} W_{mag}}{E_J - E'_J} \quad , \qquad \text{(II-19)}$$

where $E_J - E'_J$ is the energy difference between the two J levels concerned, $W_{hfs} = Am_J$, and $W_{mag} = g_J \mu_o H m_J$. The correction to A is

$$\Delta A = \frac{A^2 (I \cdot J)^2}{E_J - E'_J} \quad , \qquad \text{(II-20)}$$

where

$$I \cdot J = \frac{F(F+1) - I(I+1) - J(J+1)}{2} \quad . \qquad \text{(II-21)}$$

Both of these corrections were much smaller than the uncertainties involved in the plutonium experiment.

G. Nuclear Structure

As nuclei become heavier, collective effects become pronounced and the shell model no longer gives an adequate description of nuclear properties. The "Collective Model" of Bohr, Mottelson, and Nilsson (BOH-53, MOT-59, NIL-55) has been proposed for heavy nuclides that do not follow shell-model predictions. Nuclides described by the collective model have a larger set of angular momentum quantum numbers associated with a more complex set of motions that can include vibration and core rotation.

Figure II-4 is a diagram of the angular momentum coupling scheme for deformed nuclei, showing the relationship between the total nuclear angular momentum, $\underset{\sim}{I}$, and the vectors $\underset{\sim}{\ell}$, $\underset{\sim}{s}$, and $\underset{\sim}{R}$. Here $\underset{\sim}{\ell}$ and $\underset{\sim}{s}$ are the orbital- and spin-angular momenta of the last nucleon, and $\underset{\sim}{R}$ is the angular momentum associated with the collective rotation of the core; their components along the nuclear symmetry axis, z', are Ω, Σ, and ρ respectively. These are described in Table II-I.

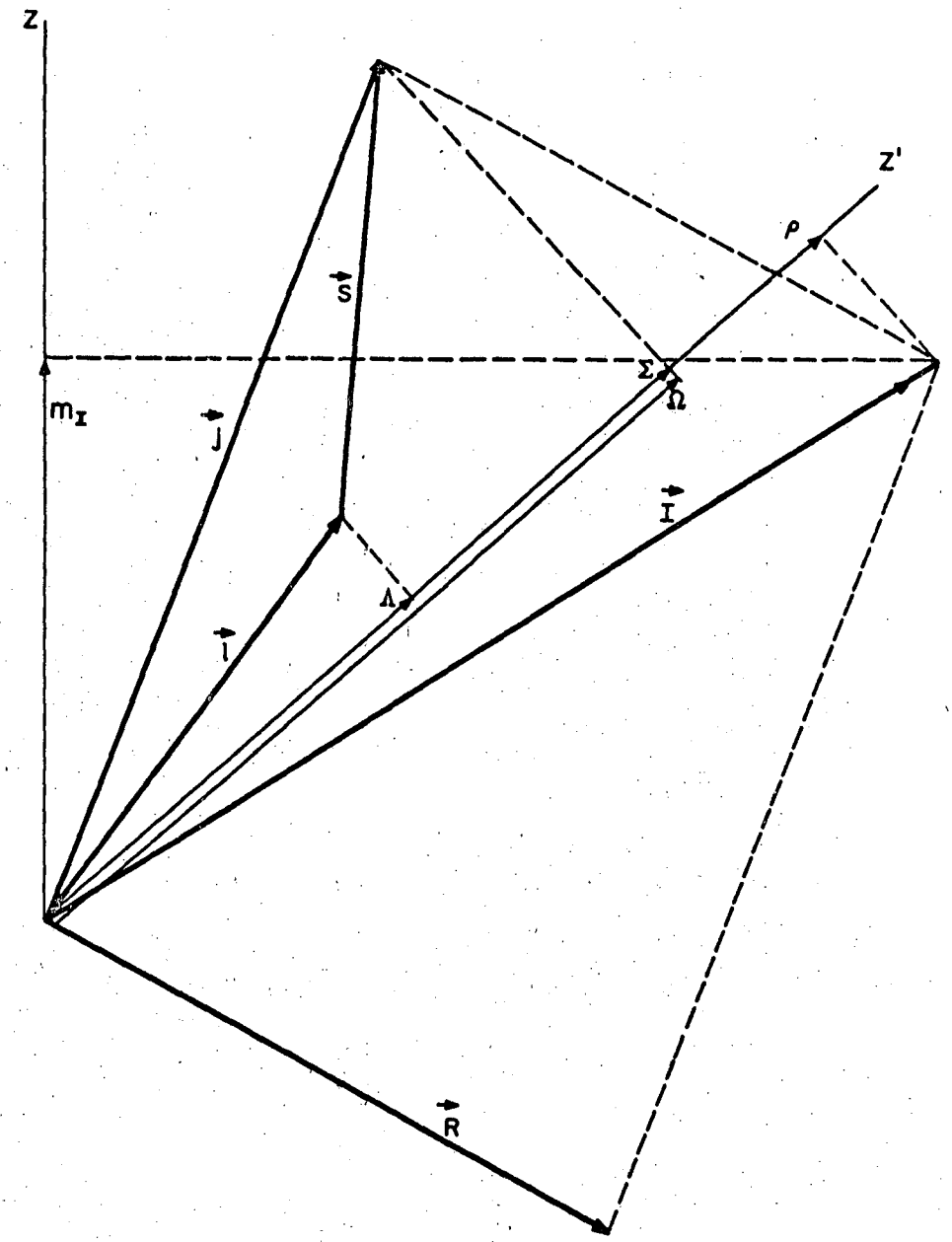

MU-16342-A

Fig. II-4 Angular momentum coupling scheme for deformed nuclei.

Table II-I. Angular momentum vectors and their components.

Angular momentum				Components	
Vector	Description			Along z	Along z'
$\underset{\sim}{\ell}$	Particle orbital				Λ
$\underset{\sim}{s}$	Particle spin				Σ
$\underset{\sim}{j}$	Particle total	=	$\underset{\sim}{\ell} + \underset{\sim}{s}$		Ω
$\underset{\sim}{R}$	Nuclear core				ρ
$\underset{\sim}{I}$	Nuclear total ("spin")	=	$\underset{\sim}{R} + \underset{\sim}{j}$	m_I	K

Note that the nuclear ground state occurs when $\rho = 0$.

The effect of collective rotation can be seen in the rotation spectrum for Pu^{239} for the ground state and three excited K-states, as shown in Fig. II-5. The symbols below each group represent the value of K and the parity; the numbers beside each line are the nuclear spin for that level. The energy for each of these levels is given by

$$E_{rot} = \frac{\hbar^2}{2\Im} \{I'(I' + 1) - I(I + 1) + a[(-)^{I'+1/2}(I' + 1/2) - (-)^{I+1/2}(I + 1/2)]\delta_{K,1/2}\} , \qquad \text{(II-22)}$$

where $\Im$ is the effective moment of inertia of the nucleus, a is a decoupling parameter which can be calculated from the wave functions of the last odd nucleon, and I' is the nuclear spin of the excited level. The parameter, a, affects only nuclei with $K = 1/2$. Values of $\Im$ and a deduced from Fig. II-5 are $\Im = 5.6 \times 10^{-50}$ g-cm^2 and $a = -0.57$. A value of $a \neq 0$ implies that $K = 1/2$.

In the strong coupling limit, when the spin orbit term can be treated as a perturbation, the good quantum numbers are Ω and π, the parity. Also, because the oscillator energy levels are well separated and the Hamiltonian couples only levels which differ by two oscillator quantum numbers, the oscillator quantum numbers N and their z' components n_z are nearly conserved and thus can be taken as good quantum numbers. The standard level nomenclature, in the strong coupling limit, is then $(N,n_z,\Lambda,\pi)_\Omega$ (NIL-55). The energy level for the ground state in Pu^{239} is characterized by $(631+)_{1/2}$, and the measured spin is indeed 1/2.

For a single odd particle outside a closed shell (odd Z) the magnetic moment is the sum of the moment of the odd particle and the moment of the core,

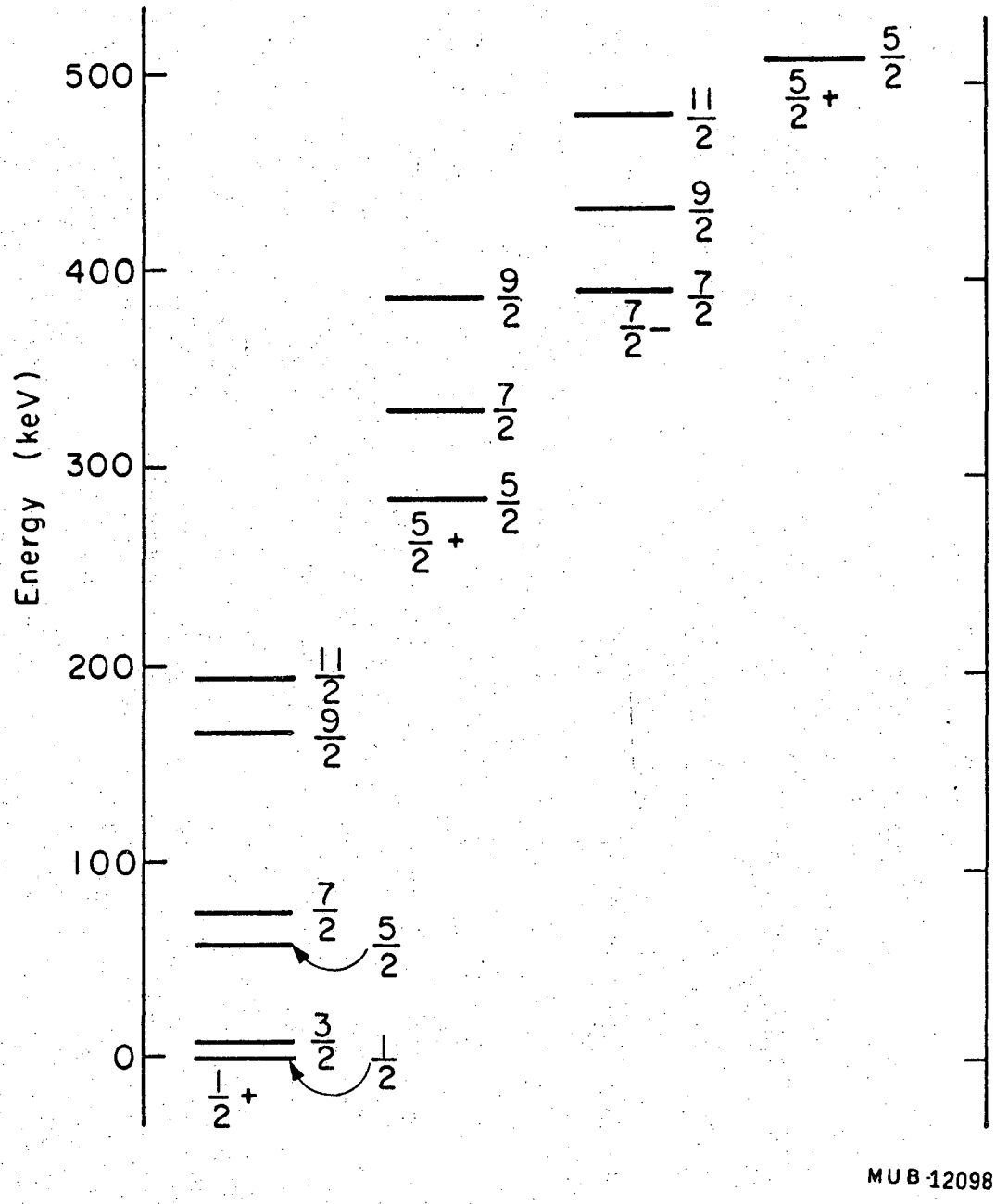

Fig. II-5 Rotational spectra for Pu^{239}.

$$\underset{\sim}{\mu} = g_s \underset{\sim}{s} + g_\ell \underset{\sim}{\ell} + g_R \underset{\sim}{R} \quad , \qquad \text{(II-23)}$$

where g_R is the g factor of the core, usually taken to be Z/A. Chiao (RAS-60) has suggested that the magnetic moments for the free proton and neutron should not be used in calculating magnetic moments of nuclei but that a "quenched" magnetic moment be used instead. The physical basis for this is that a bound nucleon has fewer virtual states to rebound into because of the closeness of the rest of the nucleons in the nuclear well. For this theory, g_s for the neutron is -2.4 and that for the proton is $+4.0$. Inglis has suggested that g_s is not unity for the proton, but 7/8, while the neutron's g_s should be 1/8 and not zero.

The nuclear Hamiltonian is

$$\mathcal{H} = \mathcal{H}_o + \zeta \underset{\sim}{\ell} \cdot s + D \underset{\sim}{\ell}^2 \quad , \qquad \text{(II-24)}$$

where

$$\mathcal{H}_o = -\frac{\hbar^2}{2M} p^2 + \frac{M}{2} (\omega_x^2 x'^2 + \omega_y^2 y'^2 + \omega_z^2 z'^2) \quad , \qquad \text{(II-25)}$$

and x', y', z' are the coordinates of each nucleon in a reference frame fixed in the nucleus. $\mathcal{H}_o$ is a simple oscillator potential to which the usual quantum mechanical spin-orbit term is added. The higher ℓ-states are reduced in energy by the ℓ^2 term. The values of ζ and D are chosen to fit empirical nuclear data (MAY-55). The Hamiltonian (II-25) can be corrected for deformation of the core by assuming a cylindrical symmetry and introducing the deformation parameter δ. In this case $\omega_x^2 = \omega_y^2 = \omega_o^2(1 + 2\delta/3)$, $\omega_z^2 = \omega_o^2(1 - 4\delta/3)$. The effect of δ on the eigenvalues of the Hamiltonian can be seen in Fig. II-6. The shell-model levels are those for $\delta = 0$. Empirical evidence for particular values

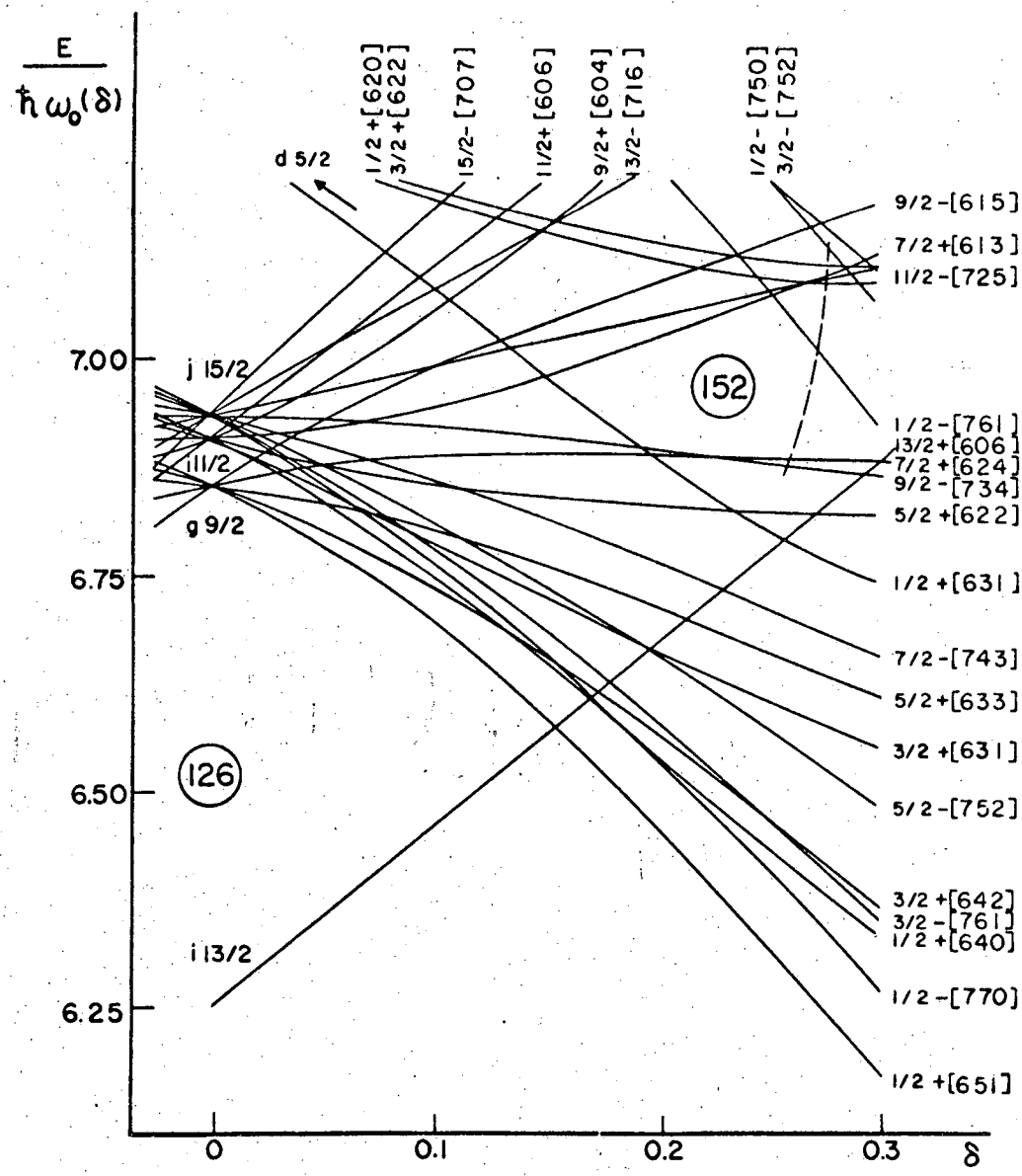

MU-15744

Fig. II-6 Neutron energy levels for N > 126.

of δ can be gotten by measuring the spin of an isotope. For instance, in Pu^{239} and Pu^{241}, the 145th and 147th neutron apparently fall into the Nilsson shells $(631+)_{1/2}$ and $(622+)_{5/2}$, respectively. The deformation parameter of about 0.26 compares favorably with the a value obtained in comparing Fig. II-5 with Eq. (II-22) for Pu^{239} (MAR-58).

H. Transition Probabilities

According to elementary quantum theory the probability that a transition between two energy levels occurs is proportional to the matrix element of a perturbing potential between the two levels:

$$P \propto |\langle \psi_{fin} | \mathcal{H}_{pert} | \psi_{in} \rangle|^2 \quad , \qquad \text{(II-26)}$$

where $\mathcal{H}_{pert} = - g_J \mu_o \underset{\sim}{J} \cdot \underset{\sim}{H}_{rf} - g_I \mu_o \underset{\sim}{I} \cdot \underset{\sim}{H}_{rf}$. Depending on the configuration of the hairpin and its position in the static C field, $\underset{\sim}{H}_{rf}$ takes on one of two forms. Either

$$\underset{\sim}{H}_{rf} = H_o \hat{k} \cos \omega t \qquad \text{or} \qquad H_o(\hat{i} \sin \omega t + \hat{j} \cos \omega t) \qquad \text{(II-27)}$$

for an oscillating rf field. Then $\mathcal{H}_{pert} = g_J \mu_o H_o J_z (e^{i\omega t} + e^{-i\omega t})/2$ or $g_J \mu_o H_o (J_+ e^{i\omega t} + J_- e^{-i\omega t})/2$, respectively.

The J_z term is diagonal in m_J while the other terms connect levels with $\Delta m_J = \pm 1$. At very low fields $P = 0$ unless $\Delta F = 0, \pm 1$ and $\Delta M = 0, \pm 1$. At very high fields, $P = 0$ unless $\Delta m_I = 0, \pm 1$ and $\Delta m_J = \pm 1, 0$ or else $\Delta m_I = \Delta m_J = 0$. The focusing force in an atomic beam apparatus is

$$F_z = - \frac{\partial \mathcal{H}_{ext}}{\partial z} \cong g_J \mu_o m_J \frac{\partial H}{\partial z} \quad , \qquad \text{(II-28)}$$

so that normally the only observable transitions are those which undergo a reversal of the quantum number m_J in the C-magnet region. These are

the transitions which (within the limitation of the selection rules above) "cross the diagram" at high fields. Such transitions have been extensively used to measure values of A, B, C, and g_J. These transitions are relatively insensitive to g_I because $g_I \ll g_J$.

In 1958 a technique was discovered (NIE-58, SAN-58) for observing transitions in an atomic beam machine which are directly dependent on g_I. Because these transitions were between levels of the same m_J, they had not been observable by previous techniques. Three independent radio-frequency loops are used to pump atoms differentially between three energy levels in the magnetic field. The energy levels are shown schematically in Fig. II-7. The atoms pass through the three loops in the order A-C-B (Fig. II-8). A normal observable transition is induced in loop A (i.e., the value of m_J is reversed). The same transition is induced in loop B, so that if nothing happens to the atom between A and B, the value of m_J is again reversed to its original value and the atom continues as if nothing had happened. No signal is observed. However, if a $\Delta m_I = \pm 1$ transition can be induced in the C loop, the frequency in the B loop will be incorrect for causing the re-reversal of m_J and the atom will continue on its way with its value for m_J the opposite of when it entered the A loop. Since this is the condition for refocusing, a signal is observed at the detector.

If the probability of inducing a transition in the A loop is P_A, then the signal strength of the A transition is

$$S_A = 2nP_A \quad , \qquad \text{(II-29)}$$

where we assume each of the hyperfine levels has an equal population of n atoms. The factor 2 occurs because atoms from each of the two possible

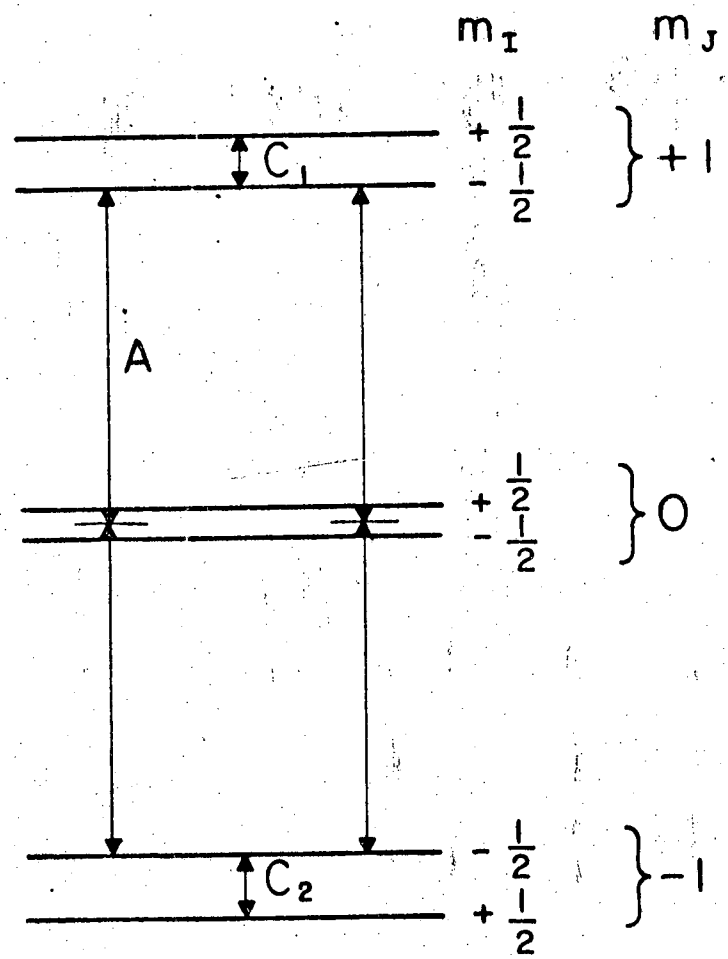

MUB 11951

Fig. II-7 Energy levels for the three-loop experiment.

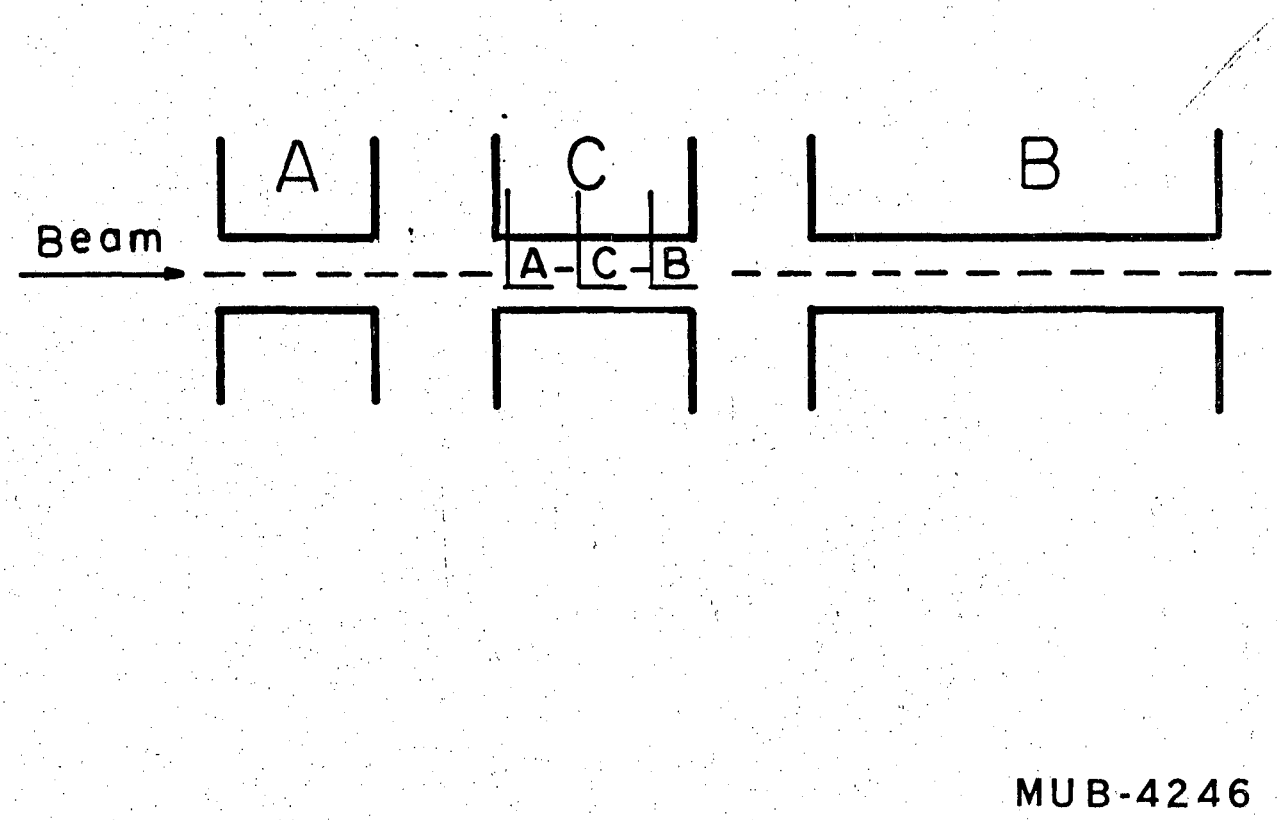

Fig. II-8 Relative orientation of the three rf loops.

paths into the C region are involved. Figure II-9 shows one of the refocused paths; the other, starting with the opposite m_J value, is symmetric to it on the opposite side of the centerline.

When the A and B transitions are induced the signal strength is

$$\begin{aligned} S_{AB} &= 2n\{(P_A - P_A P_B) + (P_B - P_B P_A)\} \\ &= 2n(P_A + P_B - 2P_A P_B) \quad . \end{aligned} \tag{II-30}$$

P_A and P_B are normally equal and near to unity so that S_{AB} is small, say 25% of S_A in the worst case.

When the effect of the C loop is considered,

$$S_{ABC} = 2n(P_A + P_B - 2P_A P_B + P_A P_B P_C) \quad . \tag{II-31}$$

For a nonzero constant value of P_A and P_B, the signal strength depends linearly on P_C.

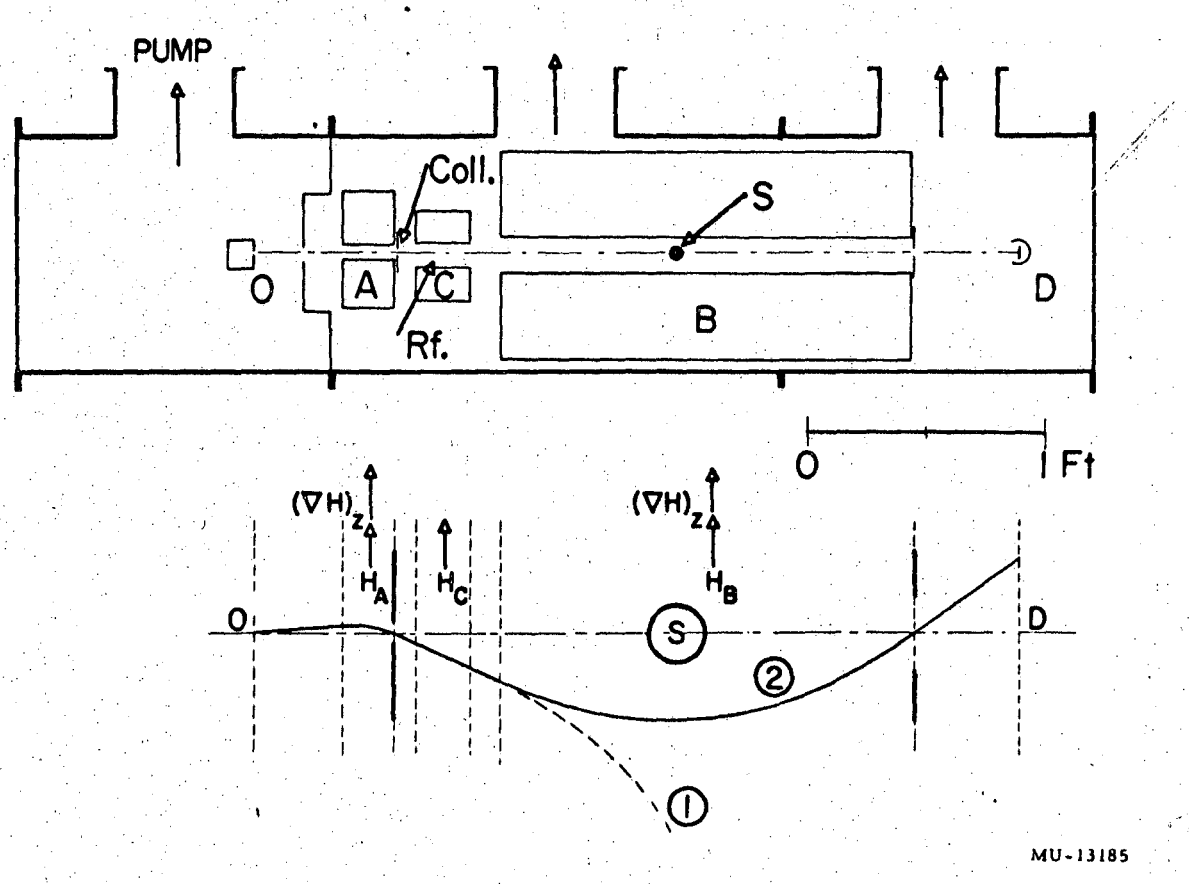

Fig. II-9 Atomic beam machine and one trajectory.

III. APPARATUS

A. Introduction

The equipment used for all the experiments described in this paper is the same as that used by White (WHI-62), except that three radio-frequency loops are used in the plutonium experiment. Minor changes in the magnet power supplies, the oven loader and buffer slits are described below as well as each of the components, for completeness.

B. Overall Design and Dimensions

The atomic beam machine used for all the experiments described in this paper (Fig. III-1) is of the unsymmetric type, with the B magnet much longer than the A magnet, resulting in a more intense refocused beam than a symmetric machine of the same total length. It is an inside-out machine with a relatively small volume which must be pumped by vacuum pumps. The A magnet is 6 in. long, the B magnet 20 in., and the C magnet 6 in. The beam traveled 58.5 in. from the source to the detector button with the new oven loader. A variable-width stop wire is in the center of the B magnet. There are collimator slits between the C and B magnets and defining detector slits on the detector side of the B magnet; the buffer chamber slits were removed to try to make it easier to see a single-quantum transition in the Pu^{241} experiment and to take full advantage of the intensity increase expected from moving the oven closer to the A magnet. The original beam flag was removed to provide room for the longer oven loader and no satisfactory replacement was made.

C. Oven Loaders and Beam Sources

Heating of the source material to an appropriate temperature to produce a vapor pressure on the order of one mm of Hg was done by electron

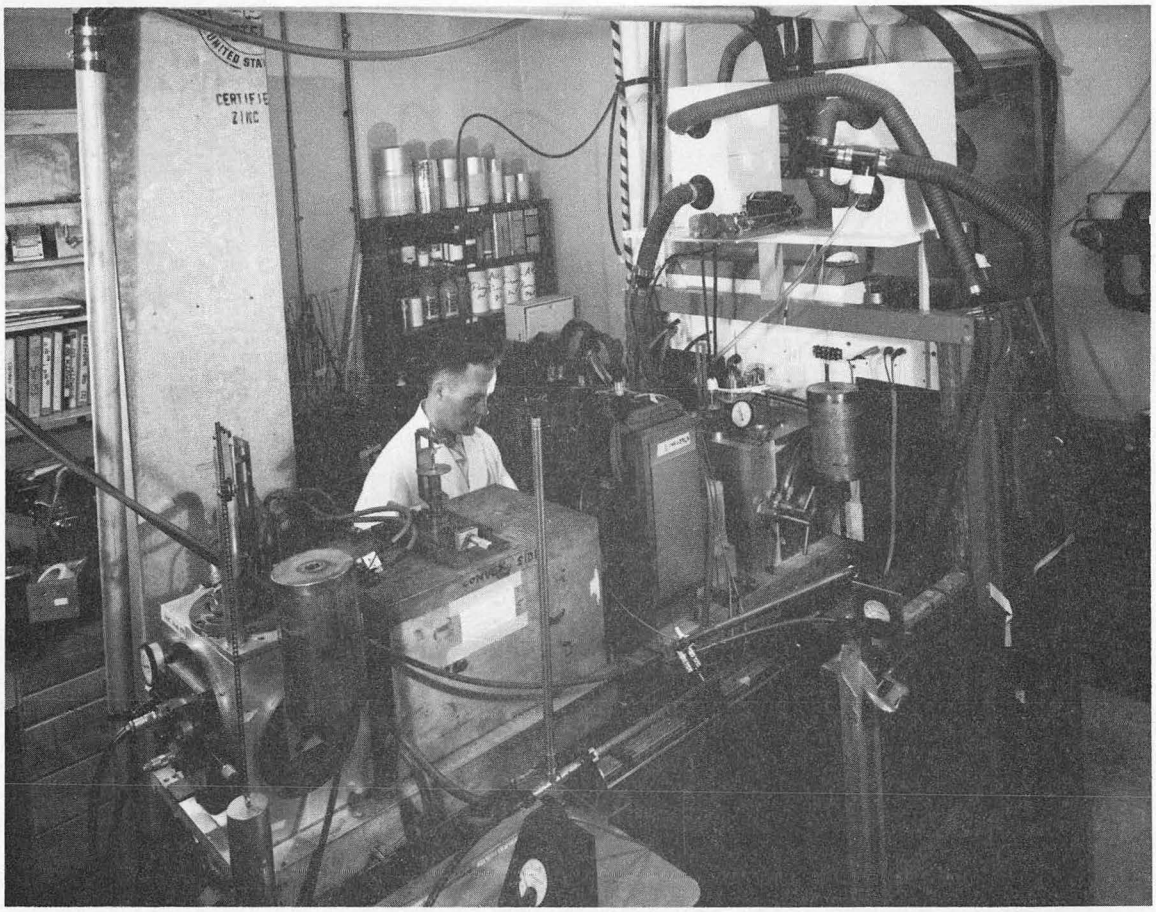

ZN-3401

Fig. III-1. Atomic beam machine.

bombardment; the electrons coming from a hot thoriated tungsten filament were attracted to an electrically positive source. In the case of the tungsten isotopes, a pure tungsten wire containing the desired isotope was placed in a holding cup and bombarded directly. The temperature was increased (by making the source more positive) to permit the oven loader to outgas until a temperature high enough to sustain a beam was achieved. The plutonium isotopes were placed inside a tungsten oven which was placed on a tantalum support plate. The oven was then bombarded with electrons.

Figure III-2 shows the most recent design of the oven loaders that was used for all parts of the experimental work done on this paper. Even though the oven-loader chamber itself was made considerably smaller and less massive in order to reduce the power needed to heat tungsten source wires to 3000°C, the added distance from the support plate produced so much torque on the stainless steel water rods that two more support rods were required to make the loader rigid enough not to sag and crack the solder joints when operating at full power.

Since the W^{187} sources were quite radioactive (> 5 curie), several features were incorporated into the loader design to minimize the time during which the experimenter had to keep his hands in close contact with the source or the parts of the oven loader that collected most of the radioactive material that boiled off from the source. The cover of the oven loader was made with a slotted hole so that it could be positioned on the loader over one of the retaining screws with remote control tongs; the other screw could then be positioned and tightened with a pair of tweezers held in the other tong. A special holder (Fig. III-3)

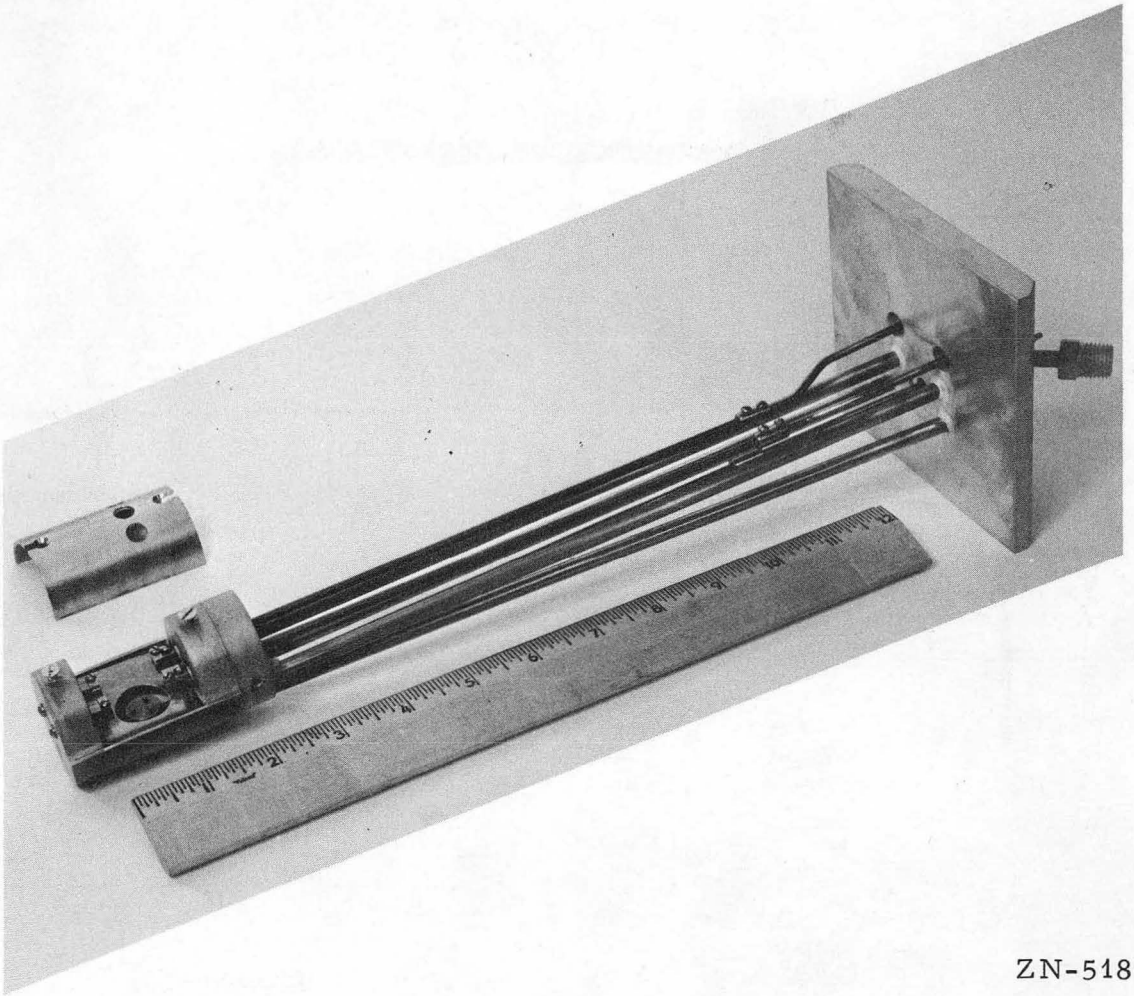

ZN-5189

Fig. III-2. Oven loader.

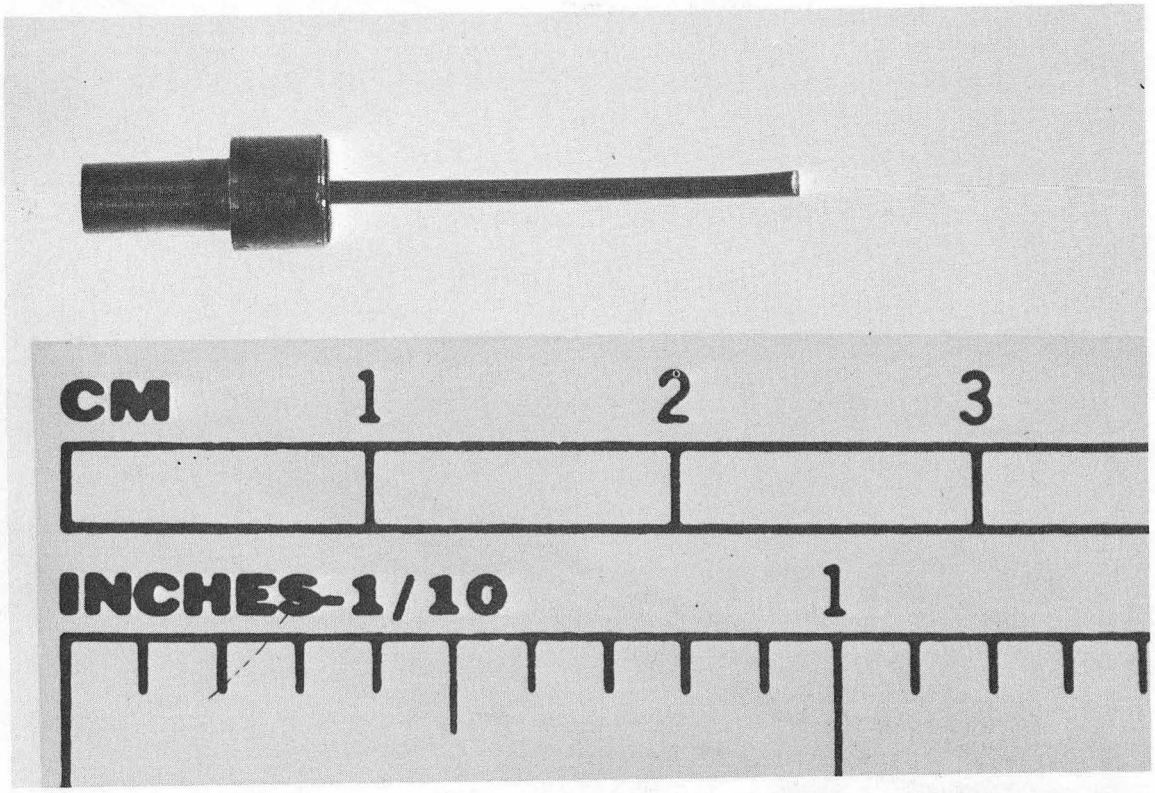

ZN-5807

Fig. III-3. Holder for tungsten source.

was designed for the tungsten-wire source so that it could be put in place with the tongs. In order to reduce the time spent on filament changing (which, even in the best of circumstances, resulted in the experimenter's receiving a large dose in the hands) the corners of the filament holder blocks were filed off so that the stiff filament ribbon would easily slide in between its block and the clamp. The outside connections for the water leads were of the quick-connect-disconnect type which required only a few seconds to attach to the support plate.

The ovens used in both of the plutonium experiments were of the usual type used for making beams of refractory isotopes: tungsten ovens with a sharp-lipped tungsten inner liner to prevent creep. However, contrary to the usual practice, tantalum slits were not welded to the oven hole since this did not seem necessary to get long-lasting beams of sufficient intensity to make a measurement of the moment.

The tungsten wire sources were heated quite close to their melting points at 1 microtorr. Consequently any slight increase in bombardment current would increase the temperature of the thin wires above their melting point, resulting in the loss of the run. A specially designed current regulator was used to prevent these fluctuations. Runs of 12 hours were not uncommon.

D. Magnet System

The "B-Magnet Power Supply" described by White was used to power both the A and B magnets simultaneously during all of the reported experiments. The C-magnet power supply used for the tungsten experiments became inoperable during the plutonium experiment, and was replaced with the old "A-Magnet Power Supply," which was better regulated even

though it could not produce so much power. The highest fields attainable in the C magnet with this power supply were only 720 gauss. The stability of the C field was also dependent on the pulsing of the Bevatron and on the stability of the line voltage. Spikes in the voltage could get past the line-voltage regulators and would sometimes cause a field change. These spikes were sometimes apparently caused by the switching of large pieces of electrical equipment in the building, so most of the precision runs in the plutonium moment measurement were done late at night and early in the morning. In addition, it was discovered that all field fluctuations were observable on a recorder which sampled the voltage across the magnet; therefore, the final run at 720 gauss was monitored continuously by the recorder. The fringe field from the Bevatron caused a field shift of about 10 milligauss (in the worst case) during the time the Bevatron field was pulsed. This resulted in an increase in intensity on the high-frequency side of the resonance line, and a decrease on the low-frequency side. This asymmetry was evident in the potassium calibrating resonances, but was not observed in the radioactive resonances because of the large statistical uncertainty in the counting rates. Nevertheless, the final plutonium run was done at a time when the Bevatron was not pulsing.

The C-magnet yoke shorted out at one stage, due to corrosion from the cooling water. While it was being rewound, the machine was found to be out of optical alignment by using a telescope lined up on the front and back of the B magnet. The only part not in line was the A magnet. In an attempt to gain greater signal-to-background ratio, the A magnet was placed back in alignment. When the new C-magnet yoke was placed

back on the machine, we were not able to see a radioactive resonance. A high enough signal-to-background ratio was finally obtained by manually moving the A magnet about until the S/B maximized. The reason for this discrepancy in position is unknown.

Since the electronic g factor for tungsten and plutonium is ≈ 1.5 whereas that of potassium is ≈ 2.0, one would expect to be able to increase the S/B by increasing the field in the A and B deflecting magnets according to the formula

$$B(x)g_J(x) = B(y)g_J(y) \quad ,$$

where B(x) is the field for an isotope with a g_J value of $g_J(x)$. The deflecting fields had been optimized for potassium, so we increased them while observing the S/B, which increased with the field until the limit of the power supply was reached.

E. Vacuum System

Two new ionization (pressure) gauges were installed, one above the buffer diffusion pump and one in the C-magnet chamber. These gauges were useful in determining the presence of very small leaks in the C-magnet region. They were also useful in eliminating high pressure along the beam path as a cause for low S/B at various times during the experiment. A manifold was installed between the main-tank mechanical pump and the main vacuum shutoff valve in order to permit helium leak detecting without having to let the whole machine up to atmospheric pressure to attach the leak detector. A cold trap which had been near the oven loader in the old design was removed when it burst and was found not repairable. Although it took longer to get the pressure to a low value, the final pressure attained was the same as when the trap was

there. Typical pressures were on the order of 0.2 to 0.5 microtorr in all parts of the machine except the oven chamber, where it was 1 to 2 microtorr. Any pressure higher than this usually indicated a leak. The mean free path (including effects of small-angle scattering which remove atoms from the collimated beam) is ≈ 30 m in the magnet and detector chamber. The total probably loss of beam under these conditions is about 10%.

The quick-change button loader used for radioactive detection continually gave serious vacuum trouble until O rings made of Viton-A synthetic rubber were used.

F. Radio-Frequency Equipment

The radio-frequency equipment used in this experiment is standard and the techniques are quite straightforward. The only difference from ordinary atomic beam magnetic resonance experiments is that three completely separate rf systems were used to power three separate rf loops (Fig. III-4).

It is possible to use a single rf loop to perform the experiment if the two frequencies involved are not too close together. Only two separate rf systems would be needed in this case. The procedure would then be to find the normal flop-in resonance with one system, then increase the power until the resonance intensity has reached a minimum. The power required to achieve this minimum, usually four to five times that needed to get an intensity maximum, can impose an intolerable demand on the rf equipment. When the minimum had been obtained, the procedure would be the same as when the minimum was obtained by using two loops; the search frequency would be varied until a resonance

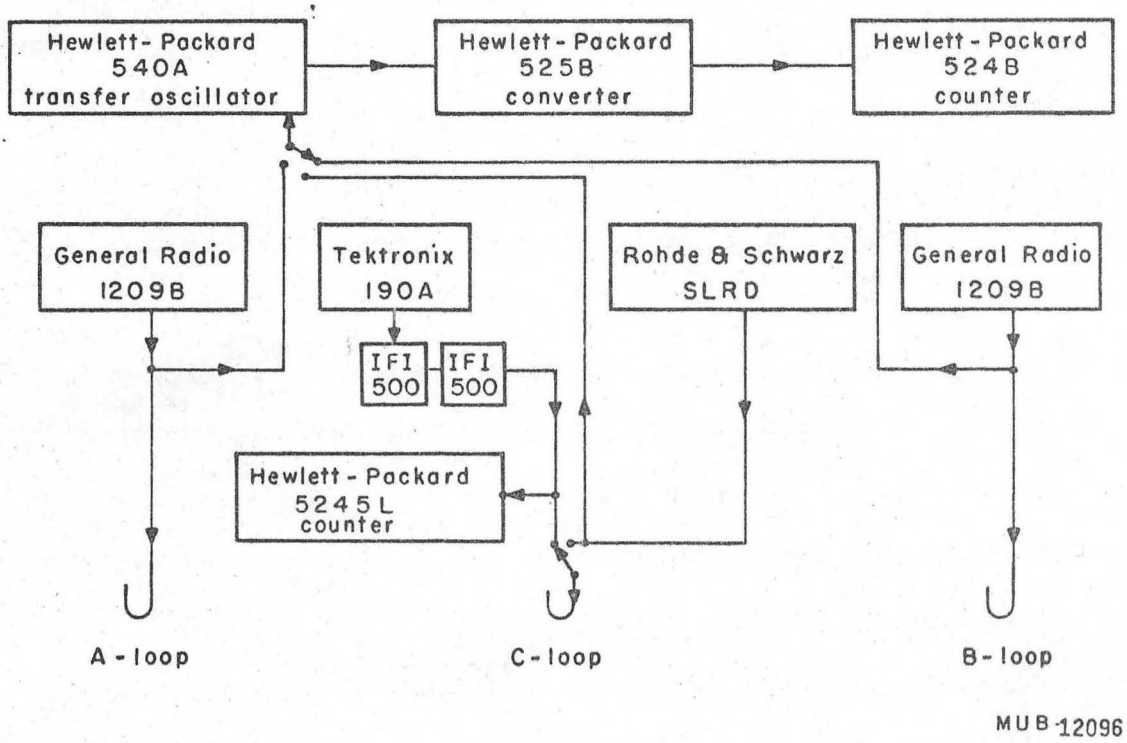

Fig. III-4 Block diagram for high-field moment search.

occurred (the search frequency is put into the same loop, along with the normal flop-in frequency, by means of an rf "tee"). The single-loop technique was not used in the plutonium experiment because of power restrictions. See Table III-I for a list of the equipment used in these experiments.

G. Detection

The resonances detected fall into two main categories according to the method of detection. The first is detection of potassium by means of a hot-wire ionization detector, and the second is detection of radioactive isotopes, which was done by depositing the beam onto platinum discs and counting the discs in continuous-flow gas counters; beta counters for the tungsten isotopes and Pu^{241}, and alpha counters for Pu^{239}.

Figure III-5 is a photograph of the machine button holder, the beta counter button holder slide, and the platinum foil discs. Figure III-6 is a schematic diagram of the head the heavily shielded beta counter used for Pu^{241}.

Hot-wire ionization detection has been treated quite thoroughly in the literature (TAY-30) and will not be further discussed here.

The aspects of radioactive detection which pertain to the tungsten experiment (beta detection) and to the Pu^{239} experiment are normal, but the detection of the β rays from Pu^{241} required some thought and experimentation. The beta spectrum of Pu^{241} has its maximum at 5 keV (SHL-56) and its end point at 20 keV. Although the usual energy of β rays detected in our counters is around 1 MeV and the lowest energies normally encountered are 100 to 200 keV, it can be shown that the counters are able to

Table III-I. Radio-frequency equipment.

Instrument	Frequency range (Mc/sec)
Oscillators:	
Tektronix 190A	0.35 to 50
Hewlett-Packard 608C	10 to 480
General Radio 1208B	65 to 500
General Radio 1209B	250 to 920
Rohde and Schwarz SLRD	275 to 2750
Hewlett-Packard 540A transfer oscillator	100 to 220
Amplifiers:	
IFI 500 wide-band amplifier	0.5 to 240
IFI 510 wide-band amplifier	0.5 to 240
Frequency-measuring instruments:	
Hewlett-Packard 524B electronic counter	0 to 10
Hewlett-Packard 5245L electronic counter	0 to 100
Hewlett-Packard 525A frequency converter	0 to 100
Hewlett-Packard 525B frequency converter	100 to 220
Hewlett-Packard 525C frequency converter	100 to 500
Hewlett-Packard 5253B frequency converter	50 to 500
Hewlett-Packard 5254A frequency converter	300 to 3000

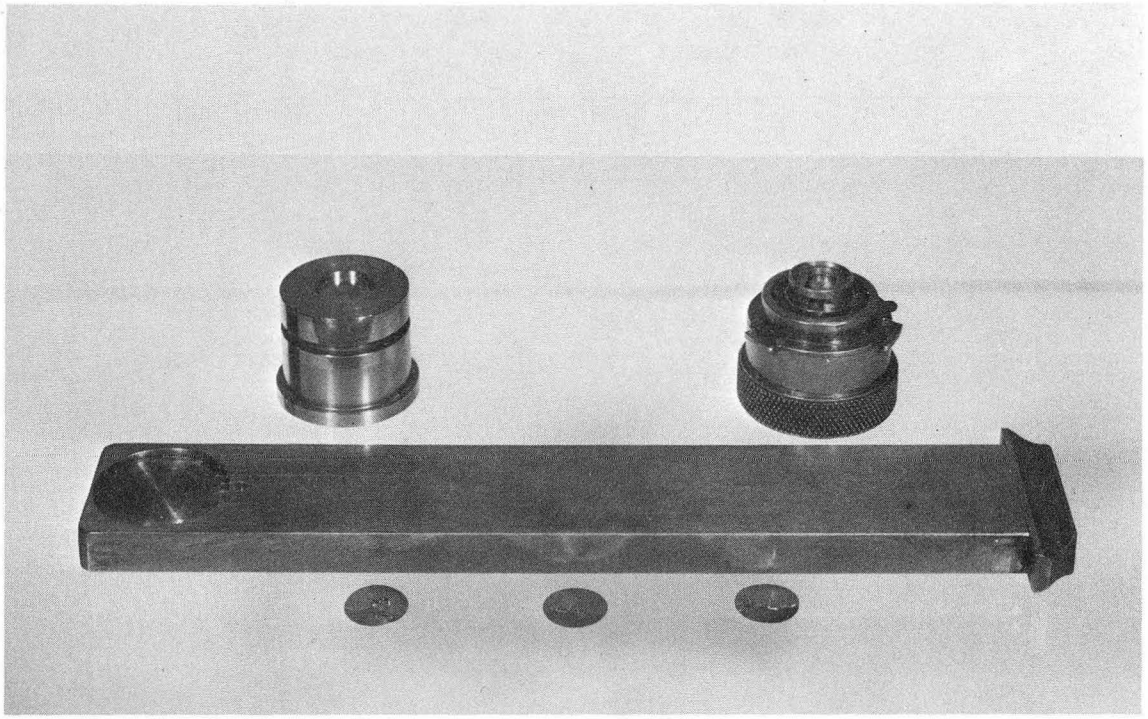

ZN-5808

Fig. III-5. Machine button holder, counter slide and holder, and platinum foil buttons.

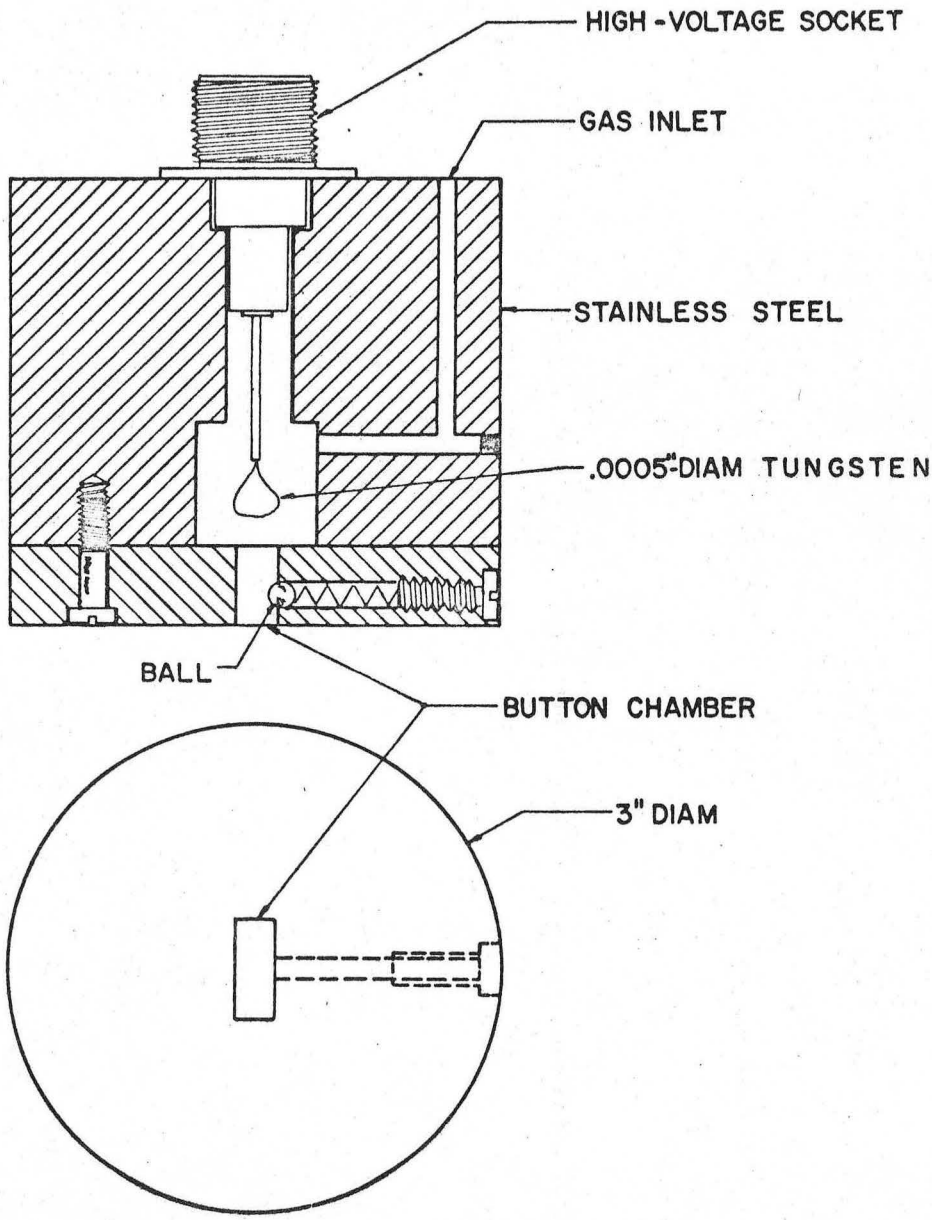

MU-17401

Fig. III-6 Counter head for continuous-flow methane counter.

respond to a 6-keV electron. (The minimum energy loss per unit length of a β particle through methane occurs at 1 MeV and is only 1.65 keV/(mg/cm^2) = 1.25 keV/cm. Assumption of a maximum path inside the chamber of 5 cm then gives the above result.) We performed an experiment which measured the counting rate of a strong beta source as a function of the amount of absorber between it and the counter. The results indicated that the counter was sensitive to betas of 5 keV and perhaps even 3 keV but no lower. Efficient use of the material would have dictated further research into improving the counting efficiency of continuous-flow methane counters in the very-low-energy range if the Pu^{241} experiment had been successful.

IV. EXPERIMENTAL PROCEDURE

A. Introduction

The experimental procedures are standard except for the triple-loop technique which will be described in detail. Other aspects are mentioned briefly.

B. Isotope Production and Handling

Plutonium-239 was obtained in high purity from the stockpile at the Lawrence Radiation Laboratory in Livermore, California. Typical experiments used from 50 to 500 milligrams of Pu^{239}. Because the allowable body burden of Pu^{239} is 1 microgram, the large amount of material needed to complete the moment measurement required extreme care in handling. All work was done in a lead-shielded Berkeley box (Fig. IV-1) with remote-control tongs. The box was kept under a lower-than-atmospheric pressure at all times to contain any radioactive material which might be loose. The isotope arrived as high-purity blocks from which chunks were chipped off (under oil) when needed. The plutonium was rinsed in toluene and placed directly into the oven for heating.

Plutonium-241 was obtained in the form of PuO_2 from Oak Ridge National Laboratory, Tennessee. Amounts of this extremely pure (94%) material no larger than a grain of sand, when mixed with large amounts of lanthanum, would give a beam of 150 to 200 cpm for 12 hours. The lanthanum, when heated, acted as a reducing agent and quite stable beams were formed.

Seventy-four-day tungsten-185 was produced from glass-encapsulated natural tungsten wires about 0.5 inch long by 20 mils in diameter,

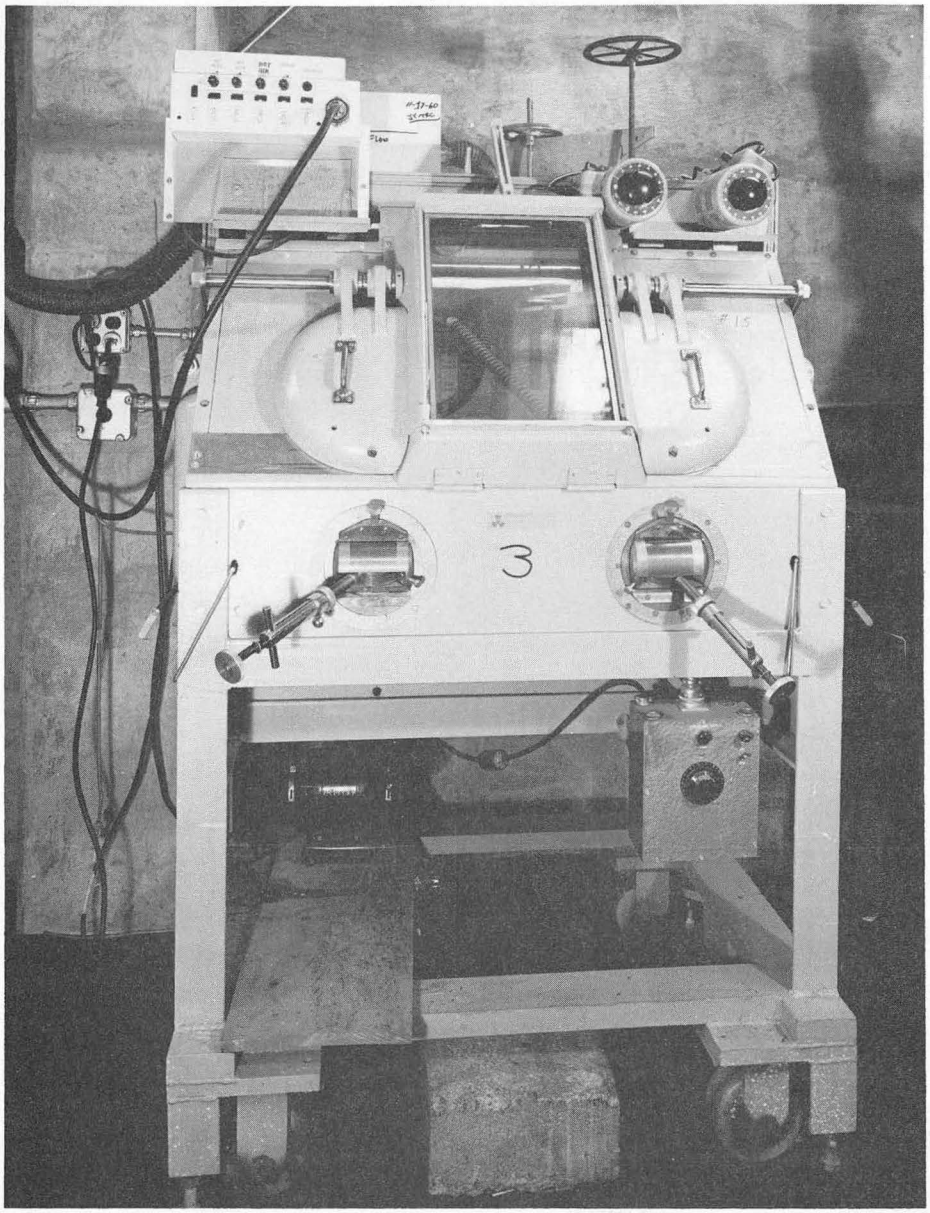

ZN-2677

Fig. IV-1. Lead-shielded gloved Berkeley box.

irradiated at the Materials Testing Reactor in Arco, Idaho. Irradiation time varied from 6 weeks to 3 months. The capsules, containing up to 20 wires each, were stored for a week after they were removed from the reactor to allow the decay of the shorter-lived W^{187}, which was produced in large amounts simultaneously. The wires were then individually dropped into the shielded cave on the oven-loading end of the machine, and placed into the oven loader with tongs.

Twenty-four-hour W^{187} was produced by irradiation at the G. E. Test Reactor in Vallecitos, California. The wires were placed into the machine and run as soon as they arrived. The W^{187} sources presented the greatest radiation hazard of any of the isotopes discussed in this paper; a hand dose of almost 100 mR was characteristic of an average run.

C. Beam Production

A schematic of an atomic beam machine has been shown in Fig. II-9. The A and B magnets act as polarizer and analyzer for atoms having trajectories that make them pass through the central C magnet region. The atoms in the beam are subjected to a force $F = g_J \mu_o m_J dH/dz$ and thus are deflected in the same direction in the B magnet as in the A (and therefore further from the center line into the magnet) unless the value of m_J changes its sign. In this case the atom is refocused back to the center line by the time it reaches the detector.

When the oven or wire (in the case of tungsten) had been lined up optically with a telescope, the source was slowly heated up while Pt foils remained in the beam path. During the first few runs, the warmup was done with all the magnets off. Periodically the foils were counted in an appropriate counter until one showed some radioactivity. After

this these "full beam" buttons were exposed for preciesly 1 minute every time the power to the source was increased, until a beam level of about 100 cpm was attained. At this point the A and B magnets were turned on and another 1-minute exposure was taken. The counting rate of this "direct beam" was compared with the previous full beam and the throwout was calculated. For the alkalis this is $\approx$ 100%; for tungsten it is 75%; for plutonium only about 30% of the beam is deflected. The information about the throwout is helpful when comparing techniques of other experimenters and in determining whether the machine is working properly whenever a resonance is not observed.

The same procedure done with the full beam buttons was repeated with the direct beam buttons until a counting rate was reached on the order of 100 cpm. The field was then set using a potassium beam, and a no-rf "resonance" button was exposed for from 5 to 15 minutes to give an indication of the background level of the machine. This was followed by a succession of direct-beam and resonance buttons. During the most precise parts of the plutonium experiment the magnetic field was checked with the potassium beam between each successive resonance-button exposure, but at other times the field was checked at intervals of only around half an hour if the field stability warranted it.

For isotopes for which the hyperfine constant is not known, such as Pu^{241} and both tungsten isotopes, one must observe resonances at low fields and follow these resonances up in field until a splitting from the Zeeman frequency occurs large enough to predict the value of the energy separation between F levels with a small enough uncertainty to warrant searching for the direct transition at low fields. The IBM 7094

computer routine HYPERFINE-4-94 is useful for determining the hyperfine separations and their uncertainties from a set of resonances at successive fields.

For plutonium-239, for which the hyperfine separation was accurately known, the procedure was different although the resonances were taken at progressively higher fields. First, on the basis of the data of Marrus et al. (MAR-58, HUB-58) a (low) field was chosen such that the uncertainty of the $\Delta m_J = 0$, $\Delta m_I = \pm 1$ transition was small enough to assure its osbervation. The field was set to this value in the central hairpin (where the field was most homogeneous) and, by means of the potassium resonance, the field at the region of the two outside hairpins was determined. The frequency that would cause the normal flop-in ($\Delta F = 0$) transition is put into the A loop, and exposures are taken while the frequency is varied until a maximum signal condition exists. Approximately the same frequency from a separate oscillator is put into the B loop (see Fig. II-8 for the relative orientation of the three loops) while the first oscillator still powers the A loop. The second frequency and power are varied until a minimum in signal strength is obtained. When both A and B hairpins have been optimized, the desired $\Delta m_J = 0$ transition frequency is introduced into the central C loop, and a resonance such as Fig. V-1 is traced out. Except for the very last and first runs, no special effort was made to adjust the signal strengths to their optimum value as long as some signal was seen. After each resonance the results of all previous runs were processed by the IBM 7094 computer routine HYPERFINE-4-94 to compute better values of $\Delta\nu$, g_I, and g_J. These values in return were used to predict the frequencies and

uncertainties at higher fields. This was continued until the highest field the power supply was capable of producing was reached. The last resonance was counted for 200 minutes total (in four counters). Typical resonances were 7 cpm when the A-B background was 4 cpm and the no-rf background was 3 cpm. Counter background was seldom as high as 0.5 cpm and the normal (single loop) flop-in transition signal strength was sometimes as high as 10 cpm. All the above signal strengths have been normalized to 15-min exposure. The maximum moment-transition signals were 0.5% of the direct beam.

V. EXPERIMENTAL RESULTS

A. Plutonium-239

Bauche and Judd (BAU-64) have analyzed the hyperfine structures of the ^7F levels in Pu-I and, by assuming a contribution to the hyperfine structure constant from configuration interaction and core polarization, conclude that the magnetic moment of Pu^{239} must be $\mu_I = 0.17(4)$ nm. Since this value is calculated from theoretical values for the fields at the nucleus, an experimental determination of the magnetic moment would be a test of this theory, as well as of the nuclear theories of the collective model.

According to the collective model (see MOT-59, p. 53, Fig. 6), a spin of 1/2 for Pu^{239} is consistent with assigning the 145th neutron to the $(631+)_{1/2}$ level with the deformation, $\delta = 0.26$. This value for the deformation (or eccentricity) parameter, δ, seems reasonable, especially since Pu^{241} has a spin of 5/2 (147th neutron in level $(622+)_{5/2}$, $\delta = 0.27$) and since the decoupling factor, a, in Eq. (II-22) can be used to calculate a value of $\delta = 0.28 \pm 0.03$ by application of Nilsson's wave functions (NIL-55). From this, Mottelson and Nilsson (MOT-59) calculate $\mu = -0.1$ nm. Use of Rasmussen and Chiao's quenched g factors and Inglis's g factors changes the magnitude of μ_I, but not its sign.

Figure V-1 shows the two $\Delta m_J = 0$, $\Delta m_I = \pm 1$ resonances observed at 720 gauss. When these resonance frequencies were combined with the data from Marrus's (MAR-58, HUB-58) hyperfine-structure data and reduced with the IBM 7094 routine HYPERFINE-4-94, we derived for the value of the magnetic moment

$$\mu_I = +0.200(4) \text{ nm (corrected)} .$$

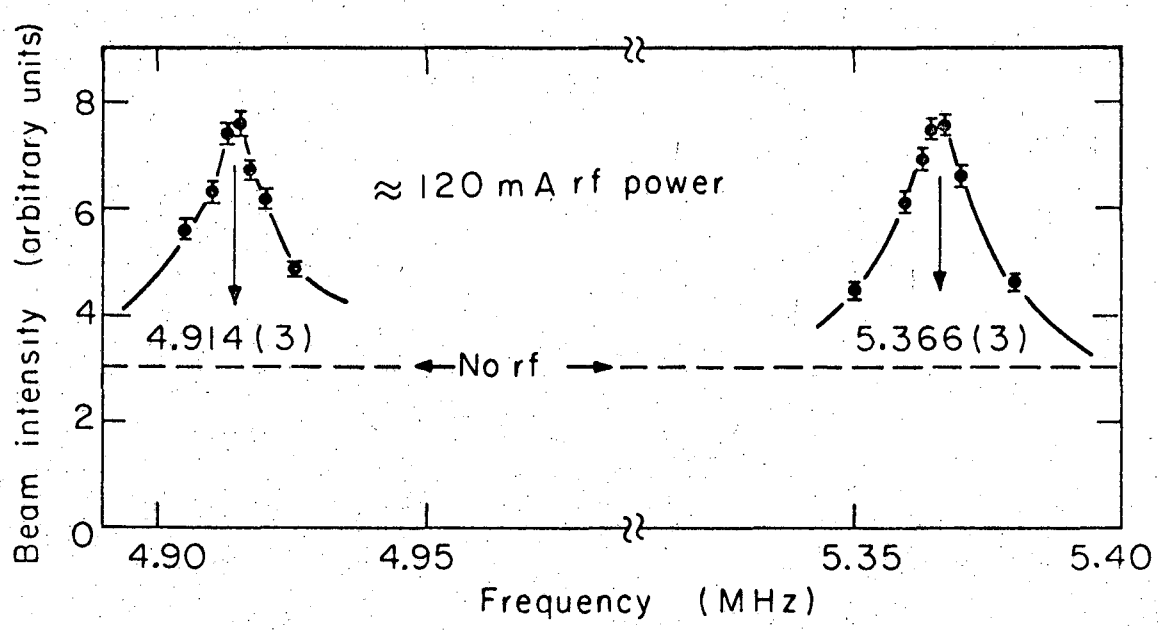

MUB 11952

Fig. V-1 $\Delta m_J = 0$, $\Delta m_I = \pm 1$ resonances at 720 gauss.

A correction for diamagnetic shielding has been made. This is a theoretical correction to reduce the effect of the electrons decreasing the magnetic field at the nucleus whenever an external magnetic field is applied. The result of the correction is to increase the value of the magnetic moment by a small amount. The correction is $\approx 1.2\%$ for $Z = 94$ (KOP-58). The data fit is shown in Table V-I. The uncertainty quoted is twice the standard deviation assigned by the computer program. Thus the experimental value is within the limits set by Bauche and Judd, but there is a lack of agreement in sign with the collective-model predictions.

B. Four- and Six-Quantum Transitions in W^{185} and W^{187}, and Pu^{241}

According to Eq. (II-15) the energy of the hyperfine levels at zero magnetic field is given by

$$E_F = \frac{1}{2} aC + \frac{b/2}{I(2I-1)J(2J-1)} [3C(C+1)/4 - I(I+1)J(J+1)] , \qquad \text{(V-1)}$$

where $C = F(F+1) - I(I+1) - J(J+1)$. There is an energy level associated with each value of F, but the relative separation and ordering of these levels depends on the value of b relative to a. Figure V-2 is a diagram of the energy level of each value of F vs b, normalized by dividing both sides of Eq. (V-1) by a, for $I = 5/2$, $J = 1$, as in Pu^{241}. More complex diagrams are obtained for W^{185} and W^{187} for the higher J-states. For the $J = 1$ state the zero-field diagram has the same shape, but the individual lines have different slopes. The important thing is that for values of $|b|$ sufficiently large, one always obtains an inversion such that the highest F level lies below one of the others. Figure V-3 is a hyperfine-energy-level diagram (schematic Breit-Rabi diagram) for

Table V-I. Fit to the Hamiltonian

$$\mathcal{H}(\text{mc}) = 5.139\ \underline{I}\cdot\underline{J} - 1.4973\ \mu_o \underline{J}\cdot\underline{H} + 2.15 \times 10^{-4}\ \mu_o \underline{I}\cdot\underline{H}.$$

Transition	H(G)	Frequency (Mc) (ν_{exp})	Residual (Mc) ($\nu_{theory} - \nu_{exp}$)
a	10.000(5)	4.445(15)	0.001
b	10.000(5)	5.688(15)	- 0.003
a	25.000(4)	4.865(15)	- 0.003
b	25.000(4)	5.385(15)	- 0.001
a	155.000(1)	5.050(15)	- 0.002
b	155.000(1)	5.220(15)	- 0.006
a	430.000(4)	4.997(10)	- 0.002
b	430.000(4)	5.276(10)	- 0.007
a	720.000(7)	4.915(20)	0.001
b	720.000(7)	5.360(20)	- 0.005
a	720.000(7)	4.914(3)	0.000
b	720.000(7)	5.366(3)	0.001

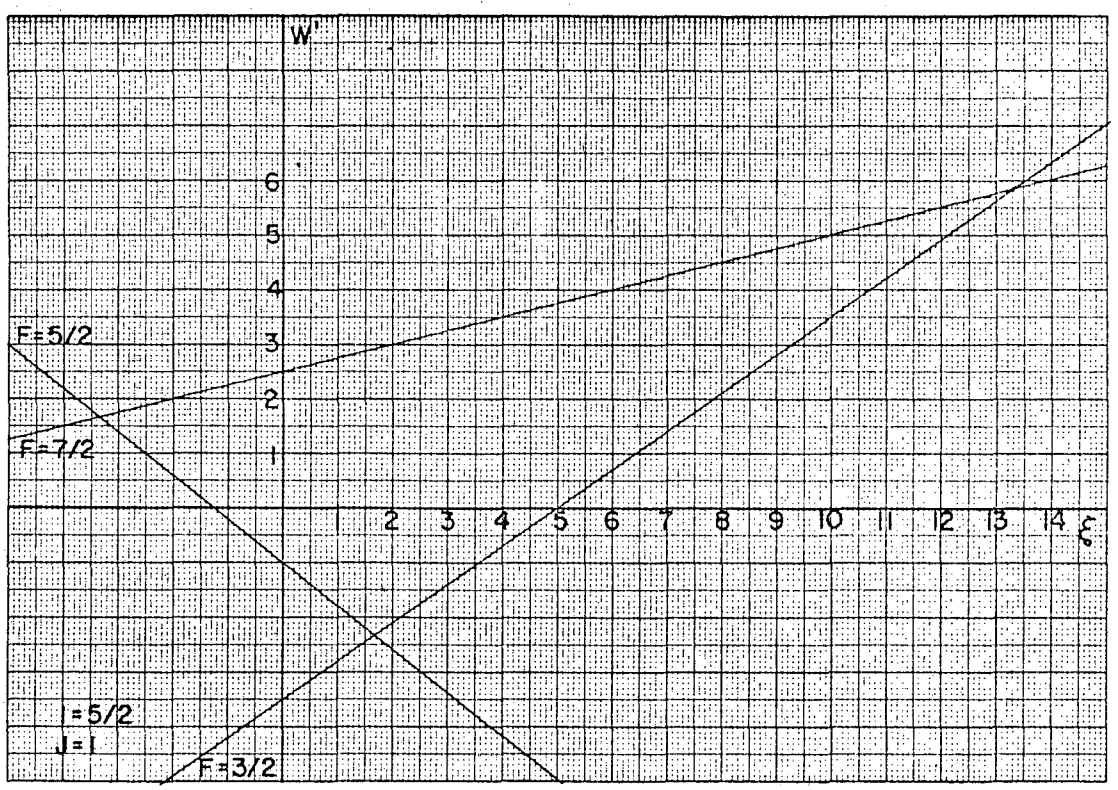

MU-21353

Fig. V-2 Zero-field energy-level diagram for Pu^{241}.

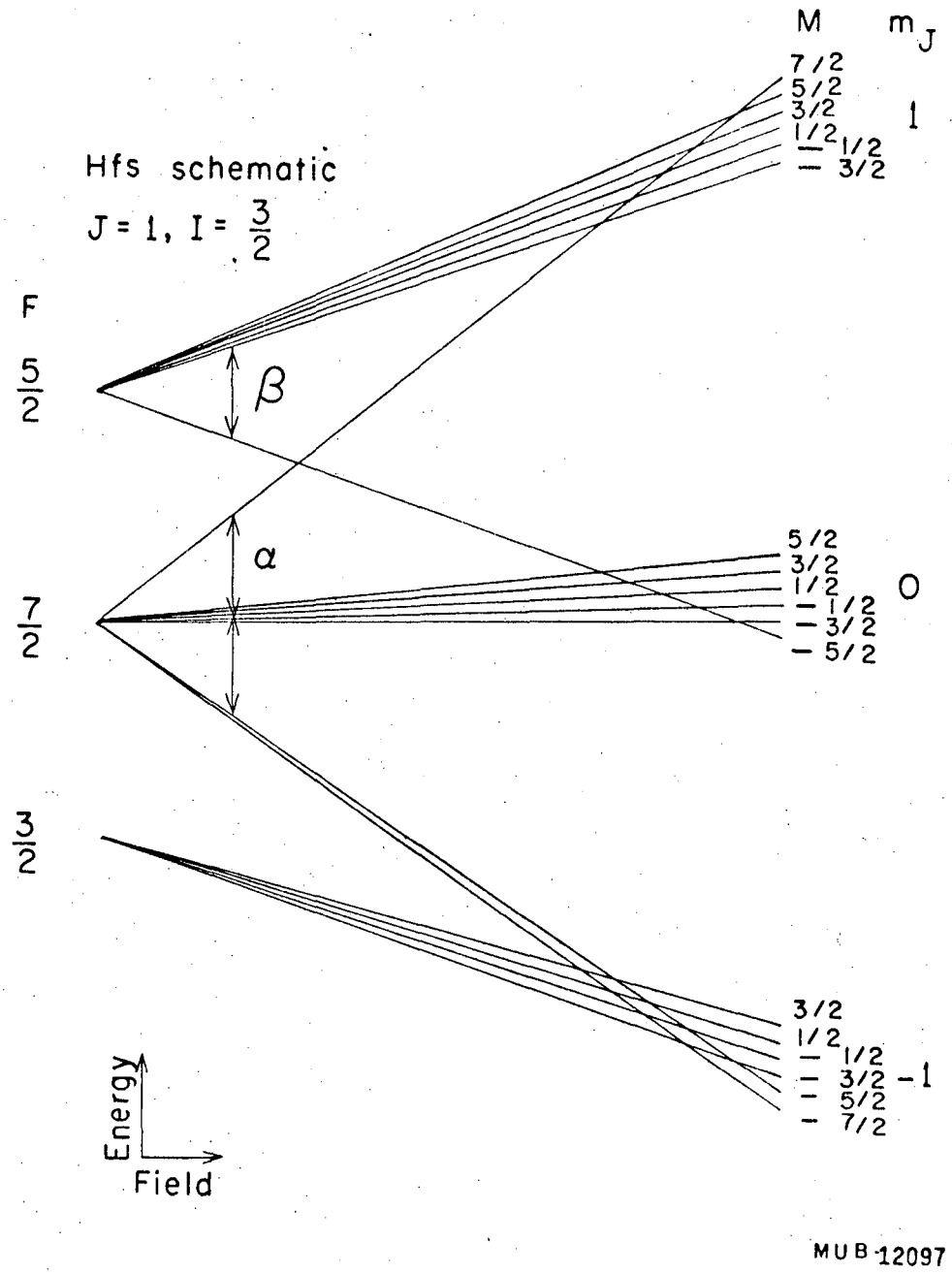

Fig. V-3 Schematic Breit-Rabi diagram for Pu^{241} if $b/a < -\frac{10}{3}$.

a value of $b < -\frac{10}{3} a$ so that the level ordering is $F = 5/2$ (highest), $7/2$, $3/2$. The only Zeeman transition possible for which refocusing can take place is the one marked α. This is a six-quantum transition; it requires six photons of the fundamental Zeeman frequency to cause the atom to jump (in six ΔM $(= \Delta m_F) = \pm 1$ steps) between the levels which are characterized by $(F,M) = (7/2, -5/2) \longleftrightarrow (7/2, 7/2)$. Figure V-4 shows that the five intermediate levels are quite evenly separated at extremely low fields, but at slightly higher fields the spacing between the $7/2$ and $5/2$ levels and between the $-3/2$ and $-5/2$ levels becomes much larger than the others. This results in a reduction in signal to the extent that at some field no resonance can be observed. No resonance for Pu^{241} was observed above 7 gauss.

In the case of the two tungsten isotopes, many resonances were observed in many J states, including $J = 4$, at many fields. As a general rule, when the field was increased the signal strength decreased. Finally, resonances were observed to disappear completely for the $J = 1$ and $J = 2$ states, and this project was abandoned.

The measured value of 5.6(2.0) b (CHA-64) for the quadrupole moment of Pu^{241} combined with the measured magnetic moment of Pu^{239} and the ratios of the moments predicts, according to a simple theory, a value of b/a of ≈ 400. The large deformations of the tungsten isotopes ($\delta > 0.2$) would indicate that they, too, have large quadrupole moments. Since the electronic state of tungsten is ^5D, one would expect small values of a, so that here, also, b/a could be large. Thus in all these cases, large values of b/a which would explain the disappearance of the resonances are theoretically probable.

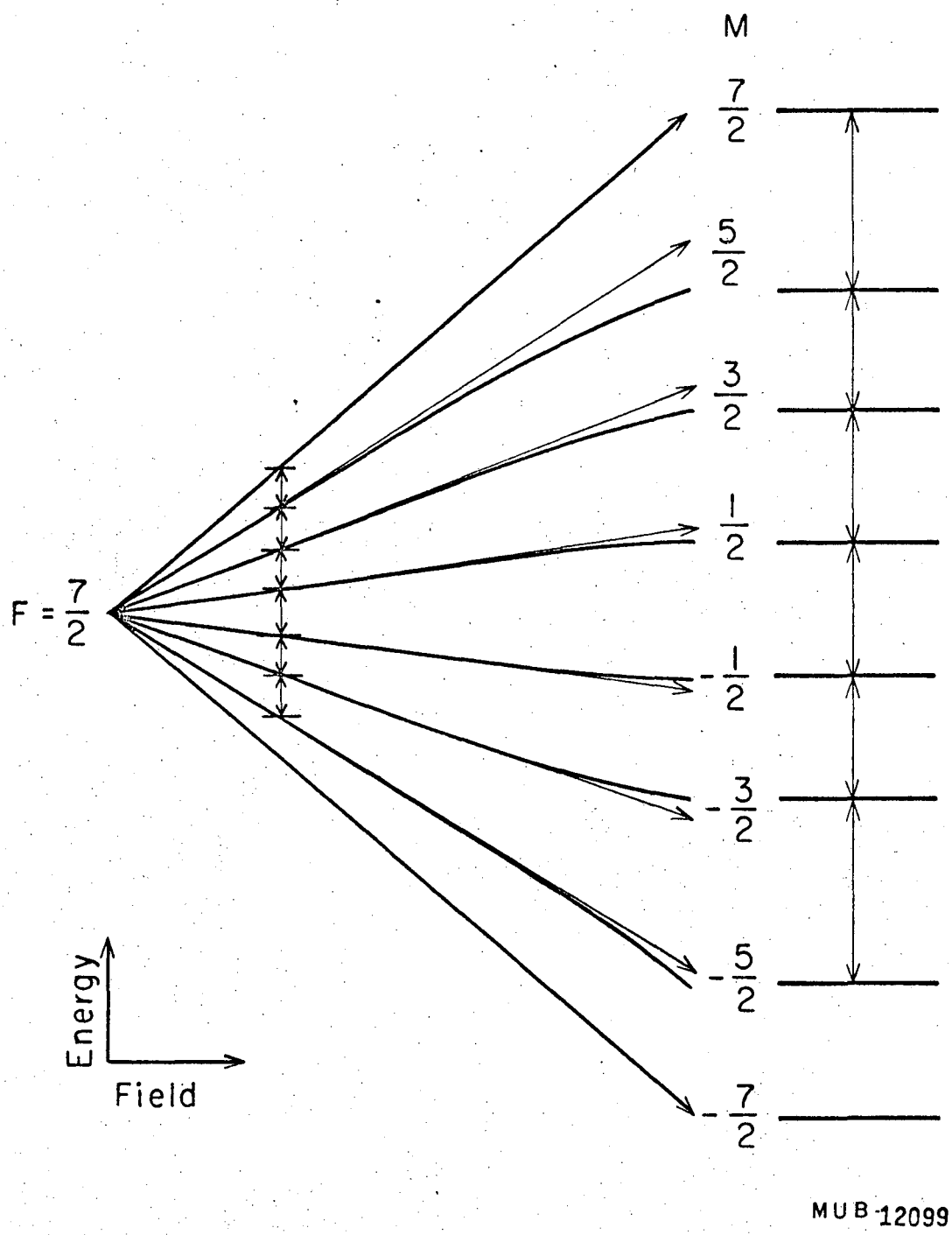

Fig. V-4 F = 7/2 level of Fig. V-3 at very low magnetic field.

ACKNOWLEDGMENTS

I wish to express my appreciation to many people who helped me complete this research: themany members of the Atomic Beam Group who discussed puzzling aspects of the work with me and all the Health Chemistry monitors who guarded my health. Especially, I would like to thank:

Professor William A. Nierenberg for his support;

Professor Richard Marrus for his guidance and encouragement;

Douglas B. Macdonald for his advice on engineering problems;

Eldred Calhoon, Betty Shipley, and especially the night monitors for handling the many radioactive samples:

Dr. Lloyd Armstrong, Jr., for his understanding when the runs ran many hours into his scheduled time;

Miss Christina Frank for typing the original and final manuscript; and

My wife, Suzanne, for keeping home, child, and husband in order during a trying time.

This research was supported by the U. S. Atomic Energy Commission.

LIST OF ILLUSTRATIONS

Fig. II-1 Relative energy splittings and degeneracies. 6

Fig. II-2 Fine, hyperfine, and magnetic splitting energy levels. . 7

Fig. II-3 Energy levels for Pu^{239} in a magnetic field. 12

Fig. II-4 Angular momentum coupling scheme for deformed nuclei . . 14

Fig. II-5 Rotational spectra for Pu^{239} 17

Fig. II-6 Neutron energy levels for $N > 126$ 19

Fig. II-7 Energy levels for the three-loop experiment. 22

Fig. II-8 Relative orientation of the three rf loops 23

Fig. II-9 Atomic beam machine and one trajectory 25

Fig. III-1 Atomic beam machine. 27

Fig. III-2 Oven loader. 29

Fig. III-3 Holder for tungsten source 30

Fig. III-4 Block diagram for high-field moment search 35

Fig. III-5 Machine button holder, counter slide and holder, and platinum foil buttons. 38

Fig. III-6 Counter head for continuous-flow methane counter 39

Fig. IV-1 Lead-shielded gloved Berkeley box. 42

Fig. V-1 $\Delta m_J = 0$, $\Delta m_I = \pm 1$ resonances at 720 gauss. 48

Fig. V-2 Zero-field energy-level diagram for Pu^{241}. 51

Fig. V-3 Schematic Breit-Rabi diagram for Pu^{241} if $b/a < -\frac{10}{3}$. . 52

Fig. V-4 $F = 7/2$ level of Fig. V-3 at very low magnetic field. . 54

LIST OF TABLES

Table I-I Other measurements of Pu^{239} 2

Table II-I Angular momentum vectors and their components 15

Table III-I Radio-frequency equipment 37

Table V-I Fit to the Hamiltonian $\mathcal{H}(mc) = 5.139\ \underline{I}\cdot\underline{J}$

$- 1.4973\ \mu_o \underline{J}\cdot\underline{H} + 2.15 \times 10^{-4}\ \mu_o \underline{I}\cdot\underline{H}$ 50

REFERENCES

BAU-64 J. Bauche and B. R. Judd, Proc. Phys. Soc. (London) 83, 145 (1964).

BER-63 C. Berthelot, J. Phys. (Paris) 24, 69 (1963).

BLE-54 B. Bleaney, P. M. Llewellyn, M. H. L. Price, and G. R. Hall, Phil. Mag. 45, 773 (1954).

BOH-53 A. Bohr and B. R. Mottelson, Kgl. Danske Videnskab. Selskab, Mat.-Fys. Medd. 27, No. 16 (1953).

BRE-31 G. Breit and I. I. Rabi, Phys. Rev. 38, 2082 (1931).

CHA-60 R.-J. Champeau and S. Gerstenkorn, Compt. Rend. 251, 352 (1960).

CHA-64 R.-J. Champeau, J. Phys. (Paris) 25, 825 (1964).

CON-35 E. U. Condon and G. H. Shortley, Theory of Atomic Spectra (Cambridge University Press, London, 1935).

GER-62 S. Gerstenkorn, Ann. Phys. (Paris) (13) 7, 367, 405 (1962).

HUB-58 J. C. Hubbs, R. Marrus, W. A. Nierenberg, and J. L. Worcester, Phys. Rev. 109, 390 (1958).

JUD-63 B. R. Judd, Operator Techniques in Atomic Spectroscopy (McGraw-Hill, New York, 1963).

KOP-58 H. Kopferman, Nuclear Moments, English version by E. E. Schneider (Academic Press, New York, 1958).

KOR-55 L. A. Korostyleva, A. R. Striganov, and N. M. Iashin, Zhur. Eksptl. i Teoret. Fiz. 28, 471 (1955); Soviet Phys.-JETP 1, 310 (1955).

KOR-62 L. A. Korostyleva, Opt. i. Spek. 12, 671 (1962): Opt. Specty. (USSR) 12, 380 (1962).

KOR-66 L. A. Korostyleva, Opt. i Spek. 20, 194 (1966); Opt. Specty. (USSR) 20, 105 (1966).

MAR-58 Richard Marrus, Hyperfine-Structure Measurements on Some Transuranic Elements (Ph.D. Thesis), UCRL-8547, November 1958.

MAR-60 R. Marrus, W. A. Nierenberg, and J. Winocur, Phys. Rev. 120, 1429 (1960).

MAY-55 M. G. Mayer and J. H. D. Jensen, Elementary Theory of Nuclear Shell Structure (John Wiley and Sons, New York, 1955).

MOT-59 B. R. Mottelson and S. G. Nilsson, Kgl. Danske Videnskab. Selskab, Mat.-Fys. Skr. 1, No. 8 (1959).

NIE-58 W. A. Nierenberg and G. O. Brink, J. Phys. Radium 19, 816 (1958).

NIL-55 S. G. Nilsson, Kgl. Danske Videnskab. Selskab, Mat.-Fys. Medd. 29, No. 16 (1955).

RAS-60 J. O. Rasmussen and L. W. Chiao, in Proceedings of the International Conference on Nuclear Structure, Kingston, Canada, ed. by Bromley and Vogt (University of Toronto Press, Toronto, Canada, 1960), p. 646.

SAN-58 P. G. H. Sandars and G. K. Woodgate, Nature 181, 1395 (1958).

SHL-56 K. N. Shliagin, Soviet Phys.-JETP 3, 663 (1956).

TAY-30 J. B. Taylor, Phys. Rev. 35, 375 (1930); see also E. Langmuir and K. H. Kingdon, Proc. Roy. Soc. (London) A107, 61 (1925).

VAN-54 M. Van den Berg, P. F. A. Klinkenberg, and P. Regnaut, Physica 20, 37 (1954); M. Van den Berg and P. F. A. Klinkenberg, Physica 20, 461 (1954).

WAT-60 R. E. Watson and A. J. Freeman, Phys. Rev. 120, 1125 (1960).

WHI-62 Matthew B. White, Hyperfine Structures and Nuclear Moments of Lu^{176m}, Br^{80}, Br^{80m}, and I^{132} (Ph.D. Thesis), UCRL-10321, September 1962.